

Structural analysis and tectonic evolution of the western domain of the Eastern Kunlun Range, northwest Tibet

Chen Wu^{1,†}, Changfeng Liu¹, Suoya Fan², Andrew V. Zuza³, Lin Ding⁴, Wencan Liu¹, Baoying Ye¹, Shijie Yang⁵, and Zhiguang Zhou¹

ABSTRACT

The Tibetan Plateau, the largest highland on Earth, formed due to the collision of India-Asia over the past 50-60 m.y., and the evolution of the Tibetan Plateau impacts our knowledge of continental tectonics. Examination of the northernmost margin of the Tibetan Plateau is key to unravelling the deformation mechanisms acting in northern Tibet. The left-slip Altyn Tagh fault system defines the northwest margin of the Tibetan Plateau, separating the Western and Eastern Kunlun Ranges in the southwest. Both Cenozoic and pre-Cenozoic crustal deformation events at this junction between the Altyn Tagh and Kunlun Ranges were responsible for the construction of northwestern Tibet, yet the relative contribution of each phase remains unconstrained. The western domain of the Eastern Kunlun Range is marked by active NE-trending, left-slip deformation of the Altyn Tagh fault and an E-striking Cenozoic thrust system developed in response India-Asia collision. To better constrain the Paleozoic Altvn Tagh and Kunlun orogens and establish the Cenozoic structural framework, we conducted an integrated investigation involving detailed geologic mapping (~1:50,000 scale), U-Pb zircon geochronology, and synthesis of existing data sets across northwestern Tibet. Our new zircon analyses from Paleoproterozoic-Cretaceous strata constrain stratigraphic age and sediment provenance and highlight Proterozoic-Paleozoic arc activity. We propose a tectonic model for the Neoproterozoic-Mesozoic evolution

 † wuchen 2016@cugb.edu.cn; wuchenlovegeology @gmail.com. of northwestern Tibet wherein restoration of an ~56-km-long balanced cross section across the western domain of the Eastern Kunlun suggests that Cenozoic minimum shortening strain was ~30% (~24 km shortening). Field evidence suggests this shortening commenced after ca. 25–20 Ma, which yields an average long-term shortening rate of 1.2–0.9 mm yr $^{-1}$ and strain rates of 4.7 × 10 $^{-16}$ s $^{-1}$ to 2.3 × 10 $^{-16}$ s $^{-1}$. Geometric considerations demonstrate that this contractional deformation did not significantly contribute to left-slip offset on the Altyn Tagh fault, which has ~10 mm/yr slip rates.

INTRODUCTION

The Tibetan Plateau is bounded by the NEstriking, left-slip Altyn Tagh fault in the northwest and three thrust systems: the NW-trending Oilian Shan in the northeast, the N-trending Longmen Shan in the southeast, and the WNWtrending Himalaya to the south (Fig. 1A). Most of the present-day topography (Fig. 1B), crustal thickness, and presently active structures were generated during Cenozoic India-Asia collision (e.g., Yin and Harrison, 2000; Tapponnier et al., 2001; Royden et al., 2008). However, preexisting structures may have played a decisive role in controlling the kinematics and dynamics of Tibetan Plateau formation. Over the past five decades, intense study of the Tibetan Plateau has led to a series of end-member models for its formation, varying from vertically uniform lithospheric shortening, lower-crustal flow, continental subduction, and convective removal of mantle lithosphere to large-scale underthrusting (e.g., Dewey and Burke, 1973; Molnar and Tapponnier, 1975; England and Houseman, 1986, 1989; Dewey et al., 1988; Royden, 1996;

Murphy et al., 1997; Clark and Royden, 2000; Tapponnier et al., 2001; DeCelles et al., 2002; Harrison et al., 1992; Zhou and Murphy, 2005; Wang et al., 2008b, 2011; Ye et al., 2015; Zuza et al., 2016, 2019).

Deformation on the major continental-scale faults in the Indo-Asian collision zone and pre-Cenozoic tectonic history figure importantly in this debate (e.g., Yin and Nie, 1996; Zhou and Graham, 1996; Sobel and Arnaud, 1999; Cowgill et al., 2003; Gehrels et al., 2003a; Pullen et al., 2008; Yin, 2010; Zhang et al., 2015; Wu et al., 2016a, 2017, 2019a; Zuza and Yin, 2017; Zuza et al., 2018, 2019; L. Wu et al., 2019c; Haproff et al., 2019). There is strong geologic evidence for numerous pre-Cenozoic collisional events that undoubtedly influenced how the Cenozoic Himalayan-Tibetan orogen evolved from initial India-Asia collision, including in the Kunlun and Altyn Tagh Ranges (e.g., Jolivet et al., 2001; Sobel et al., 2001), Karakoram-Pamirs in the west (e.g., Fraser et al., 2001; Robinson et al., 2003), Qilian Shan in the north (e.g., Wu et al., 2017; Liu et al., 2018, 2019; Zuza et al., 2018, 2019), Songpan-Ganzi in the east (e.g., Roger et al., 2011; Zhan et al., 2018), and Lhasa and Qiangtang terranes in the south (e.g., Murphy et al., 1997; Ding and Lai, 2003; Kapp et al., 2005, 2007). Detailed knowledge of the initial lithospheric conditions prior to India-Asian collision, including the existence of any precollisional topography in Tibet (e.g., England and Searle, 1986; Kong et al., 1997; Murphy et al., 1997; Kapp et al., 2005, 2007; Liu-Zeng et al., 2008; Yang and Liu, 2009; Xiao et al., 2009, 2012; Zuza et al., 2019), is required to quantify Cenozoic deformation and advance our understanding of continental tectonics.

These tectonic models make specific predictions for the deformation history, location, and

GSA Bulletin; https://doi.org/10.1130/B35388.1; 12 figures; 1 table; Data Repository item 2019388.

¹Structural Geology Group, China University of Geosciences (Beijing), Beijing 100083, China

²Department of Earth and Atmospheric Sciences, University of Houston, Houston, Texas 77204, USA

³Nevada Bureau of Mines and Geology, University of Nevada, Reno, Nevada 8957, USA

⁴Institute of Tibetan Plateau Research, Chinese Academy of Sciences, P.O. Box 9825, Beijing 100085, China

⁵Exploration and Development Research Institute of PetroChina, Liaohe Oilfield Company, Panjin 124000, China

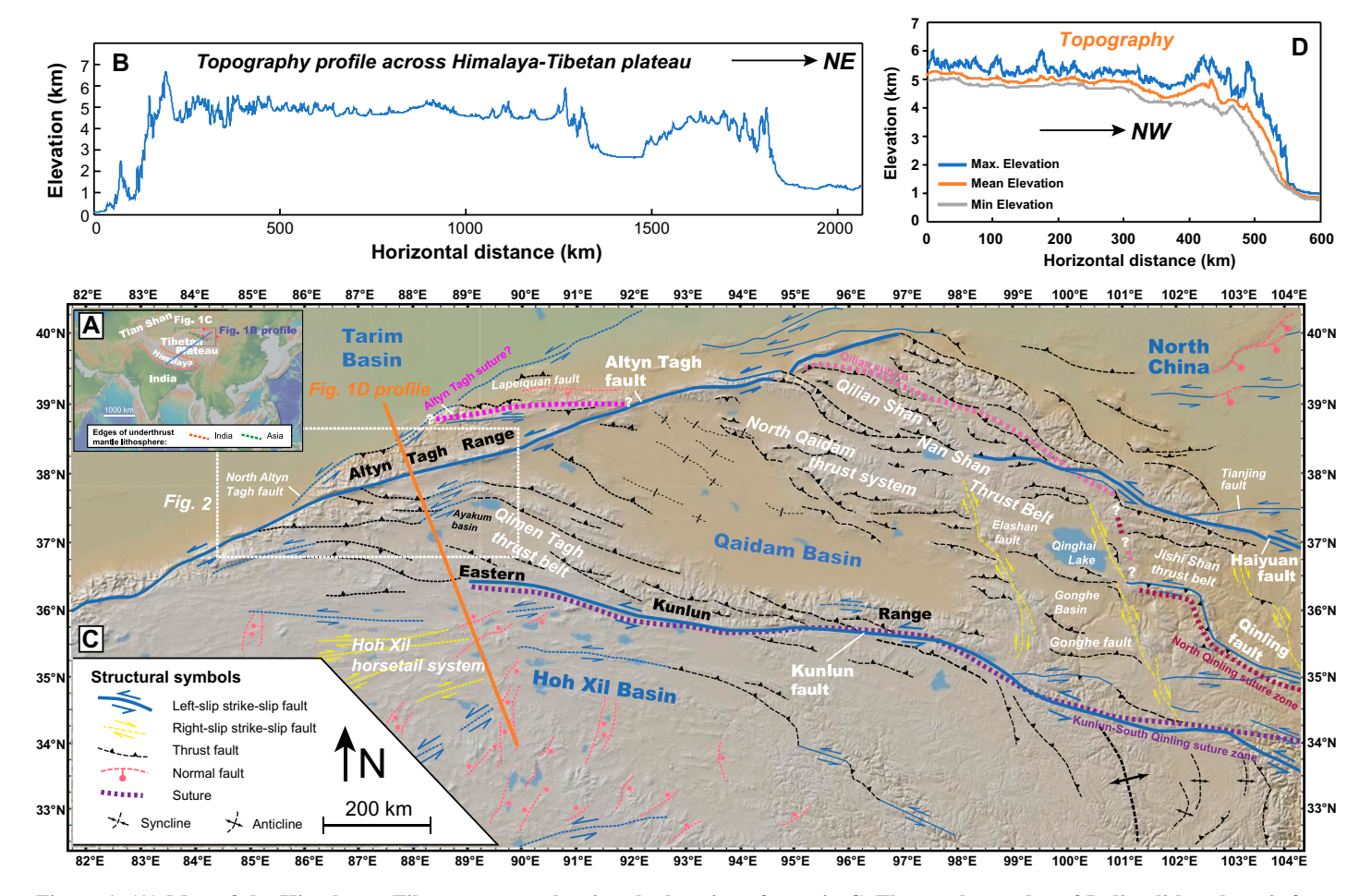


Figure 1. (A) Map of the Himalayan-Tibetan orogen showing the location of map in C. The northern edge of Indian lithosphere is from Nábělek et al. (2009), and the southern edge of Asian lithosphere is from Ye et al. (2015). Blue line shows 2000-km-long profile for topography plots in B. (B) Topography along the 2000-km-long profile across the Himalayan-Tibetan orogen. (C) Map of Cenozoic regional tectonics in northern Tibet based on Burchfiel et al. (1991), Gaudemer et al. (1995), Yin and Harrison (2000), Taylor and Yin (2009), Zuza et al. (2016), Wu et al. (2019a), and Zuza et al. (2019). Also shown is approximately 600-km-long profile (orange line) for topography plot in D. (D) Topography along the 600-km-long swath profile across the northwestern Tibet. The blue and gray lines encompass the maximum and minimum values in the swath profile, respectively.

kinematics of crustal structures, and the strain distribution in north Tibet (e.g., Meyer et al., 1998; Lease et al., 2012; F. Cheng et al., 2017a; Zuza and Yin, 2016, 2018). The last few decades have witnessed prolific research across north Tibet, focusing on the style, magnitude, and timing of continental-scale fault deformation, including the Altyn Tagh fault system (e.g., Wang, 1997; Yin et al., 2002; Cowgill et al., 2000, 2004; Mériaux et al., 2004, 2005; Cowgill, 2007; Zhao et al., 2006; L. Wu et al., 2019c), the ~1000-km-long Kunlun left-slip fault (e.g., Fu et al., 2005; Yuan et al., 2013; Duvall et al., 2013; Clark et al., 2010; Zuza and Yin, 2016, 2017; Wu et al., 2019a, 2019b), and Qilian Shan thrust system (e.g., Duvall et al., 2011; Wu et al., 2017; Ye et al., 2015; Zuza and Yin, 2016, 2017; Zuza et al., 2016, 2018, 2019; Wang et al., 2019). The active, left-slip Altyn Tagh fault system defines

the northwest margin of the Tibetan Plateau; at its northeastern end, the fault links with thrust belts in the Nan Shan–Qilian Shan, separating the Western and Eastern Kunlun Ranges in the southwest (Fig. 1C). Interpretations of the relative roles of Cenozoic versus pre-Cenozoic crustal deformation at the junction between the Altyn Tagh and Kunlun Ranges have also been proposed for the construction of northwestern Tibet; however, the kinematic picture and pre-Cenozoic tectonic history are less clear in this region.

To address some of these issues, we conducted an integrated geologic field and analytical study involving detailed geologic mapping (~1:50,000 scale), structural analysis, sedimentology, and geochronology across the western domain of the Eastern Kunlun Range, near the Cherchen and Aksu River Valleys in the Xinjiang

and Qinghai Provinces of western China. This study is unique because it may juxtapose Qilian suture structures (i.e., northwest of the Altyn Tagh fault) against Kunlun suture (i.e., southeast of the Altyn Tagh fault) structures. Our interdependent goals were to (1) establish the structural framework and quantify the magnitude of Cenozoic crustal shortening across the junction of the Altyn Tagh and Kunlun fault systems, and (2) improve our understanding of the pre-Cenozoic geology of northwestern Tibet and specifically provide new constraints on the Paleozoic Altyn Tagh and Kunlun orogens.

GEOLOGIC FRAMEWORK

The northwestern Tibetan Plateau has an average elevation of ~4.0 km, and this high topography decreases rapidly to <1.0 km in the Tarim

Basin to the northwest (Fig. 1D). The northwestern boundary of the Tibetan Plateau is presently the left-slip Altyn Tagh fault and western part of the Eastern Kunlun thrust belt, which is also referred to as the Qimen Tagh thrust belt (Fig. 1C). These Cenozoic features overprint complex geological relationships that include Paleozoic orogeny and Mesozoic extension. The brief discussion below is concerned primarily with the geology of Altyn Tagh and Eastern Kunlun Ranges.

Altyn Tagh Range

The Altyn Tagh Range marks the northwestern margin of the Tibetan Plateau, separating the Tarim Basin in the north from the Tibetan Plateau in the south. Lithologically, the Altyn Tagh Range consists of Archean and Proterozoic metamorphic gneisses along its northeastern edge, whereas Precambrian marble, schist, and quartzofeldspathic gneisses dominate in the west. The Altyn Tagh Archean metamorphic complex together with the Archean-Paleoproterozoic complex of the northeast margin of the Tarim Basin are considered to be the basement of the Tarim craton (Xinjiang BGMR, 1993; Che and Sun, 1996). Proterozoic stromatolite-bearing sedimentary sequences, consisting mostly of thickly bedded quartzite and cherty limestone, are present in the central and eastern range (Xinjiang BGMR, 1993; Chen et al., 2003). Early Paleozoic volcanic and marine sediments are exclusively exposed in the eastern Altyn Tagh Range; they are apparently absent in the western part of the range. Coal-bearing Jurassic continental sediments are also scattered throughout the Altyn Tagh Range, whereas Cretaceous strata are only exposed in the southwestern edge of the range east of Qiemo (Xinjiang BGMR, 1993; Cowgill et al., 2000, 2004; Chen et al., 2003).

Two E-trending early Paleozoic suture zones have been proposed at the northeastern and southwestern portions of the Altyn Tagh Range; both typically consist of sparse ultramafic fragments and are laterally discontinuous (Fig. 1C; e.g., Che et al., 1995; Sobel and Arnaud, 1999; Yin and Harrison, 2000; Chen et al., 2003). They were both highly modified by the subsequent Mesozoic and Cenozoic deformation (Chen et al., 2003). The Early-Middle Cambrian to Early Silurian (ca. 524-437 Ma) mélange zone is ~10-50 km wide and extends from Hongliugou eastward to Lapeiquan for ~200 km (e.g., Guo et al., 1999; Liu et al., 1999; Zhang et al., 2001, 2008; Xiu et al., 2007; Yang et al., 2008; Liu et al., 2009, 2012). It is bounded by the Altyn Tagh Archean basement to the north and the Mesoproterozoic and Neoproterozoic block to the south (Liu et al., 2009). Phengite and paragonite separated from blueschist and eclogite within the mélange complex yielded consistent ³⁹Ar-⁴⁰Ar ages of 512–491 Ma (Zhang et al., 2005). An early Paleozoic subduction-collision complex (ca. 510–445 Ma) outcrops principally in the southwestern Altyn Tagh and extends 250 km from west of Mangnai to south of Qiemo (e.g., Liu et al., 1998). The high-pressure/ultrahigh-pressure metamorphic rocks of this complex have metamorphic ages of ca. 510–480 Ma and Neoproterozoic protolith ages of ca. 1000–750 Ma (Liu et al., 1998, 2007, 2009; Liu et al., 1999; Zhang et al., 1999, 2004, 2005).

Numerous early Paleozoic granitoid plutons are exposed throughout the north Altyn Tagh region. These plutons have been assigned ages ranging from 500 Ma to 405 Ma, divided into three stages: (1) 500-480 Ma island-arc magmatism related to oceanic crust subduction (e.g., Qi et al., 2005; Wu et al., 2006, 2009; Kang et al., 2011); (2) 475-445 Ma syncollision magmatism (e.g., Wu et al., 2006, 2009; Hao et al., 2006), with the exception of a ca. 443 Ma porphyritic granite pluton that is related to the continental margin subduction event (Chen et al., 2003); and (3) 435-405 Ma calc-alkaline magmatism related to postcollisional extension (e.g., Qi et al., 2005; Wu et al., 2006, 2009). Late Cambrian-Silurian granitic plutons (491-414 Ma) sporadically occur in the south Altyn Tagh region (e.g., Sobel and Arnaud, 1999; Xinjiang BGMR, 1993; Dong et al., 2011). The apparent absence of Neoproterozoic and late Paleozoic granitoids in the south Altyn Tagh Range, as reported in regional geologic maps and published papers, is most likely a result of the lack of detailed geologic studies.

Mesozoic regional extension is thought to have affected much of northern Tibet (e.g., Vincent and Allen, 1999; Chen et al., 2003; Yin et al., 2008a, 2008b; Zuza et al., 2016, 2108), which is expressed by the development of extensive Jurassic and Cretaceous extensional and transtensional basins. Early Paleozoic muscovite ⁴⁰Ar/³⁹Ar ages from the footwall of Cretaceous normal faults at the southwestern Altyn Tagh Range indicate that the magnitude of Cretaceous normal faulting was relatively minor (<~10 km; Chen et al., 2003).

The ~600-km-long Altyn Tagh Range lies within the Cenozoic Altyn Tagh fault system as a tectonic sliver (Figs. 1C and 2; Yin and Harrison, 2000; Cowgill et al., 2000, 2004; Dupont-Nivet et al., 2004; Cowgill, 2007). The active, left-slip Altyn Tagh fault system (Molnar and Tapponnier, 1975; Meyer et al., 1996; Wang, 1997; Rumelhart et al., 1999; Bendick et al., 2000; Ritts and Biffi, 2000; Cowgill et al., 2000, 2003, 2004; Cowgill, 2007; Yin et al., 2002; Yue et al., 2005, 2004; Mériaux et al., 2004; Zhao et al.,

2006; L. Wu et al., 2019c) is the largest strikeslip system in Asia-it lies along the northwest margin of the Tibetan Plateau and extends from the Cherchen fault in the northwest to the Altyn Tagh fault, ~100 km to the southeast (Fig. 2; e.g., Cowgill et al., 2004). The left-slip Altyn Tagh fault defines the southern edge of the Altyn Tagh Range and appears to have initiated by ca. 49 Ma (Yin et al., 2002). The North Altyn fault separates the Altyn Tagh Range to the south from the Tarim Basin to the north (Cowgill et al., 2000), and its western end is dominated by left-slip motion with a subsidiary component of thrusting (Fig. 2). The Cherchen fault is a steeply dipping, left-slip structure that strikes parallel to the Altyn Tagh fault (Fig. 2) and mostly cuts Paleozoic through Quaternary rocks (e.g., Cowgill et al., 2004; Zhao et al., 2006).

Eastern Kunlun Range

The Eastern Kunlun Range, with an average elevation of ~5000 m, consists of Precambrian gneisses, Ordovician to Triassic arc assemblages, and scattered Jurassic to Cenozoic continental strata (e.g., Harris et al., 1988; Mock et al., 1999; Yin and Harrison, 2000; Cowgill et al., 2003; Robinson et al., 2003; Roger et al., 2003; Pan et al., 2004; Bian et al., 2005; Lu and Xiong, 2009; Wu et al., 2016a, 2019a, 2019b; Yu et al., 2017; Dong et al., 2018). The Precambrian basement was intruded by Ordovician to Silurian (some to Late Devonian), and Permian to Triassic arc sequences, including the prominent Permian-Triassic Kunlun batholith exposed in the Eastern Kunlun Range (e.g., Cowgill et al., 2003; Robinson et al., 2003; Gehrels et al., 2003a; Mo et al., 2007; Chen et al., 2012; Li et al., 2015; Wu et al., 2016a, 2019a; Lu et al., 2017). U-Pb zircon ages of Phanerozoic plutonic rocks across the Eastern Kunlun Range comprise two distinct groups: 290-195 Ma and 490-375 Ma. Neoproterozoic granitic gneisses are scatted within the eastern and western ends of the range (see a summary and references in Wu et al., 2016a, 2019a). Late Devonian to early Carboniferous shallow-marine strata may have been deposited during back-arc extension between the arc events (Yin and Harrison, 2000). The Triassic Yidun arc, bounding the eastern side of the Songpan-Ganzi terrane, is the eastern extension of the Permian-Triassic Kunlun batholith and is locally intruded by Cretaceous (ca. 105-95 Ma) granites (Reid et al., 2005; C. Wu et al., 2016a). Scattered Jurassic to Cenozoic continental strata overlie the highly folded Triassic strata across the Eastern Kunlun Range (Pan et al., 2004). At the western end of the Eastern Kunlun Range, a Cretaceous (74 ± 3 Ma) pluton has also been documented (Robinson et al., 2003).

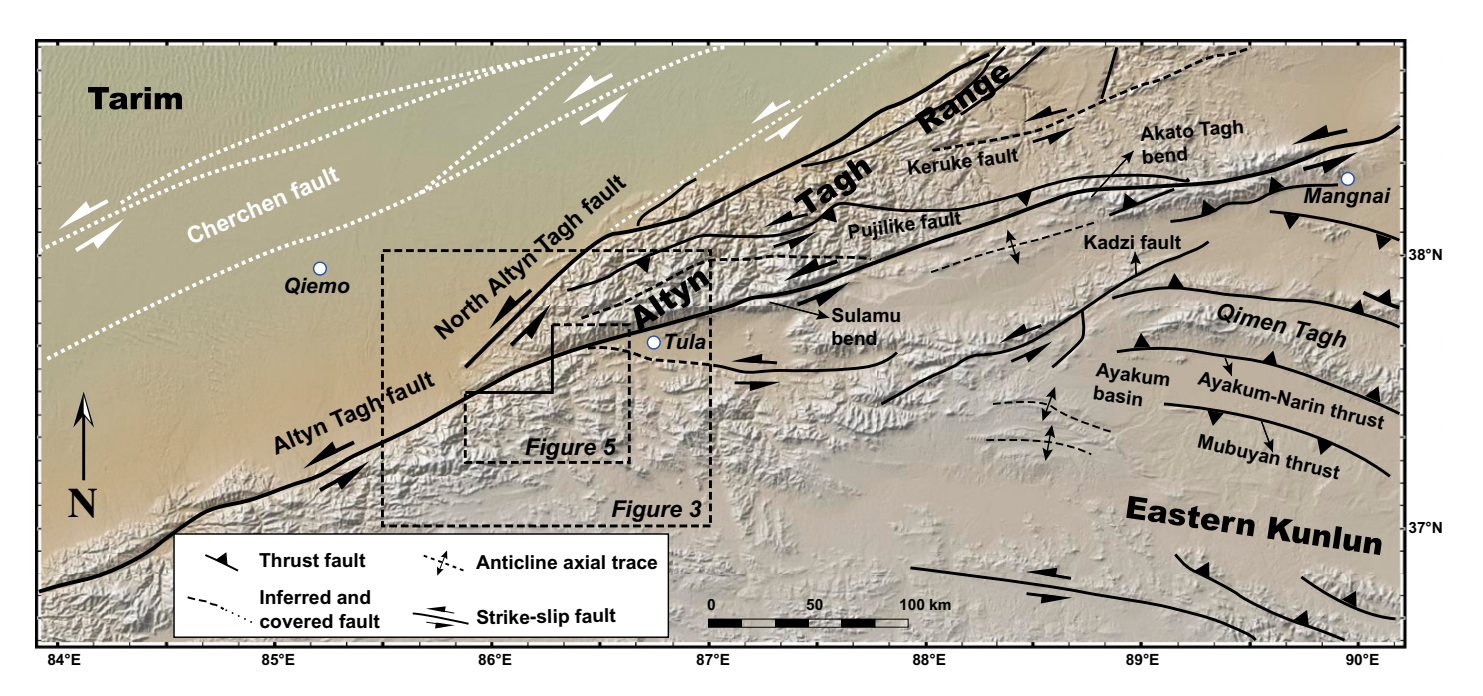


Figure 2. Regional tectonic map of the western domain of the Eastern Kunlun Range and its adjacent regions (modified from Cowgill et al., 2004). Major faults are denoted with black lines. Underlying base map is from www.geomapapp.org (Ryan et al., 2009).

Tectonically, the Eastern Kunlun Range forms a large transpressional fault system, consisting of the E-trending, left-slip Kunlun fault that merges with the WNW-trending Qimen Tagh and Bayanhar thrust belts (Fig. 1C; e.g., Yin and Harrison, 2000; Fu et al., 2005; Fu and Awata, 2007; Yin et al., 2008a, 2008b; Duvall et al., 2013; Yuan et al., 2013; Li et al., 2016, 2018). The thrust belts show a remarkable symmetry with respect to the Kunlun fault, both having a triangular shape and widening away from the central segment of the Kunlun fault (Yin and Harrison, 2000; Zuza and Yin, 2016). The Kunlun fault terminates in the west at WNWtrending thrusts and N-trending rifts (Yin et al., 1999; Yin and Harrison, 2000; Jolivet et al., 2003; Zuza and Yin, 2016) and in the east at the N-trending Longmen Shan thrust belt (Arne et al., 1997; Li et al., 2016). Clockwise rotation has defined northern Tibet's deformation for most of the Cenozoic (Zuza and Yin, 2016). Although earthquakes occur in the Western Kunlun Range at mantle depths of >70 km (e.g., Kidd and Molnar, 1988; Jolivet et al., 2003; Fu et al., 2005; Tocheport et al., 2006; X.G. Cheng et al., 2017b), they are entirely restricted to the upper and middle crust in the Eastern Kunlun Range (e.g., Chu et al., 2009), with thrust and strike-slip mechanisms (Chen et al., 1999; Zhu et al., 2006). Cenozoic tectonic models of the Eastern Kunlun Range all emphasize the presence of a major S-dipping, range-bounding thrust, which links with the Qilian Shan thrust belt via a S-dipping detachment (Burchfiel et al., 1989; Chen et al.,

1999). However, field studies have so far failed to recognize such a structure (e.g., Zhu and Helmberger, 1998; Pan et al., 2004; Yin et al., 2007, 2008b). Less is known about the Cenozoic shortening across the Eastern Kunlun Range, although Yin et al. (2007, 2008b) documented >30 km of shortening (>30% strain) across some of the northern ranges of the Qimen Tagh thrust system at the western margin of the Eastern Kunlun Range (Fig. 1C).

In the western domain of the Kunlun fault system, the wall rocks on the south side of the fault host a series of splaying structures that include linked left-slip and extensional faults, commonly defining elongate pull-apart basins bounded by NNE-striking normal faults (Fig. 1C; e.g., Jolivet et al., 2003; Yin, 2000). Initial field work along the northwestern margin of the Eastern Kunlun Range indicated that the contact between Cenozoic sediments of the Qaidam Basin and the Paleozoic bedrock of the Kunlun Range is depositional (Yin et al., 2007). Seismic reflection profiles across the southern Qaidam Basin indicated that the dominant structures are S-directed thrusts, carrying Qaidam Basin strata with an average elevation of ~2800 m in their hanging wall as a large piggyback basin (Yin et al., 2008b). All major thrusts across the Eastern Kunlun Range north of the Kunlun fault are S-directed, with only one exception, i.e., the Mubuyan thrust (Fig. 2). Some of the thrusts are linked with Estriking, left-slip faults subparallel to the Kunlun fault or terminate at NW-striking, left-slip faults of the Altyn Tagh fault system (Fig. 2). As an example, the ~100-km-long, ENE-striking Kadzi fault is a left-slip fault located in the northwestern Eastern Kunlun Range (Fig. 2), which branches from the Altyn Tagh fault at a slightly oblique angle and likely accommodates a portion of left-slip along the Altyn Tagh fault system (Cowgill et al., 2004).

GEOLOGY OF THE WESTERN DOMAIN OF THE EASTERN KUNLUN RANGE

Detailed field observations during this study focused on the junction between the Kunlun and Altyn Tagh along the southern Cherchen River (Fig. 3). The river valley, at elevations of ~3000 m, is bounded by approximately NE-trending ranges with moderate relief. The goal in focusing on this location was to relate Cenozoic deformation across the western domain of the Eastern Kunlun Range to provide an integrated view of the development of the northern Tibetan Plateau.

Stratigraphic age assignments of the major lithologic units are primarily from Pan et al. (2004) and Wang et al. (2013), and the more detailed framework used in this study is based on Xinjiang BGMR (1993) and our own field observations (Fig. 4). Lithostratigraphic units range in age from Paleoproterozoic and Mesoproterozoic to Quaternary, and they are described below. Specifically, more detailed geologic mapping (~1:50,000 scale) and structural analysis were conducted along the Aksu and Qiemo Rivers,

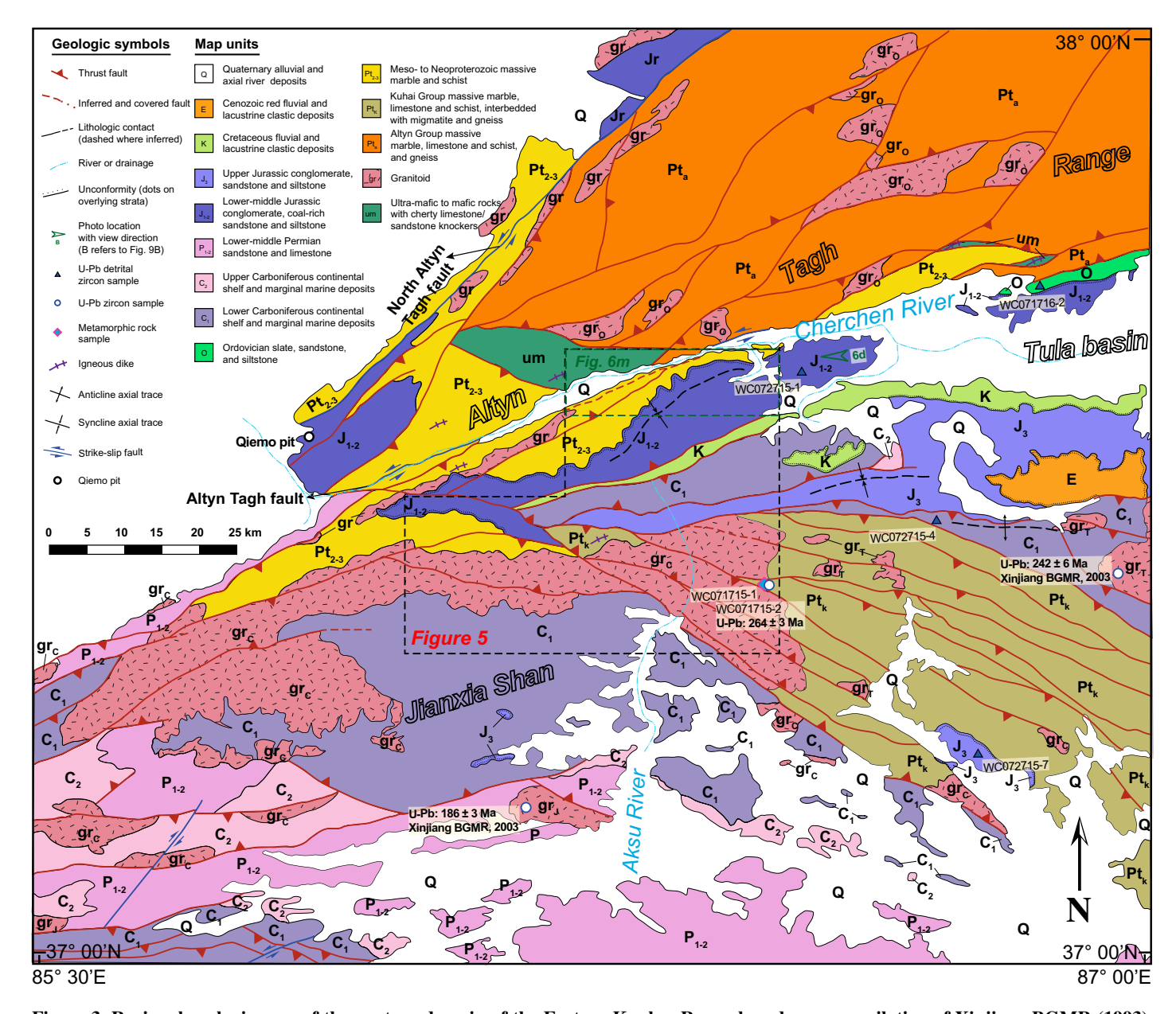


Figure 3. Regional geologic map of the western domain of the Eastern Kunlun Range based on a compilation of Xinjiang BGMR (1993), Xinjiang BGMR (2003), and our own geologic mapping and structural interpretations. The map units are from a tectonostratigraphic scheme presented in Figure 4; location is shown in Figure 2.

which drain the Tibetan Plateau to the north and east (Fig. 5). The Qiemo River is a southern tributary of the Cherchen River.

Metamorphic Basement and Sedimentary Units

Metamorphosed basement rocks (labeled Pt_a in the Altyn Tagh Range or Pt_k along the Aksu River in Fig. 3) are widespread in the mapping area and were divided into three unit groups from older to younger: gneiss, metavolcanic, and paraschist (Xinjiang BGMR, 2003). The gneiss unit is composed of quartzofeldspathic gneiss,

mylonitic biotite orthogneiss, and paragneiss. These rocks are inferred to be Paleoproterozoic in age based on previous geologic maps (e.g., Qinghai BGMR, 1991b105b105b104b147b146; Pan et al., 2004). An \sim 2 km migmatite layer was developed within the gneiss unit (Fig. 6A). The metavolcanic unit consists of gray-green metaultramafic and mafic rocks, and foliated garnet amphibolite. The paraschist is characterized by mica \pm garnet schist, quartzite, marble and local limestone, and local phyllite and slate; these rocks have been interpreted as part of a Proterozoic passive margin. Metamorphosed basement rocks are characterized by mica quartz schist,

marble, and local limestone. Slightly foliated Paleozoic granitoid rocks intrude both the carbonate and schist units.

The oldest sedimentary strata (labeled Pt₂₋₃) exposed in the western domain of the Eastern Kunlun Range consist of massive-bedded limestone and schistose quartz sandstone. The carbonate rocks have a distinct massive blue/gray appearance. The stratigraphic thickness of this unit probably exceeds ~3 km but is poorly constrained because its basal contact with the underlying metamorphosed basement is not observed, and internal deformation has affected the original stratigraphy. The regional geologic map

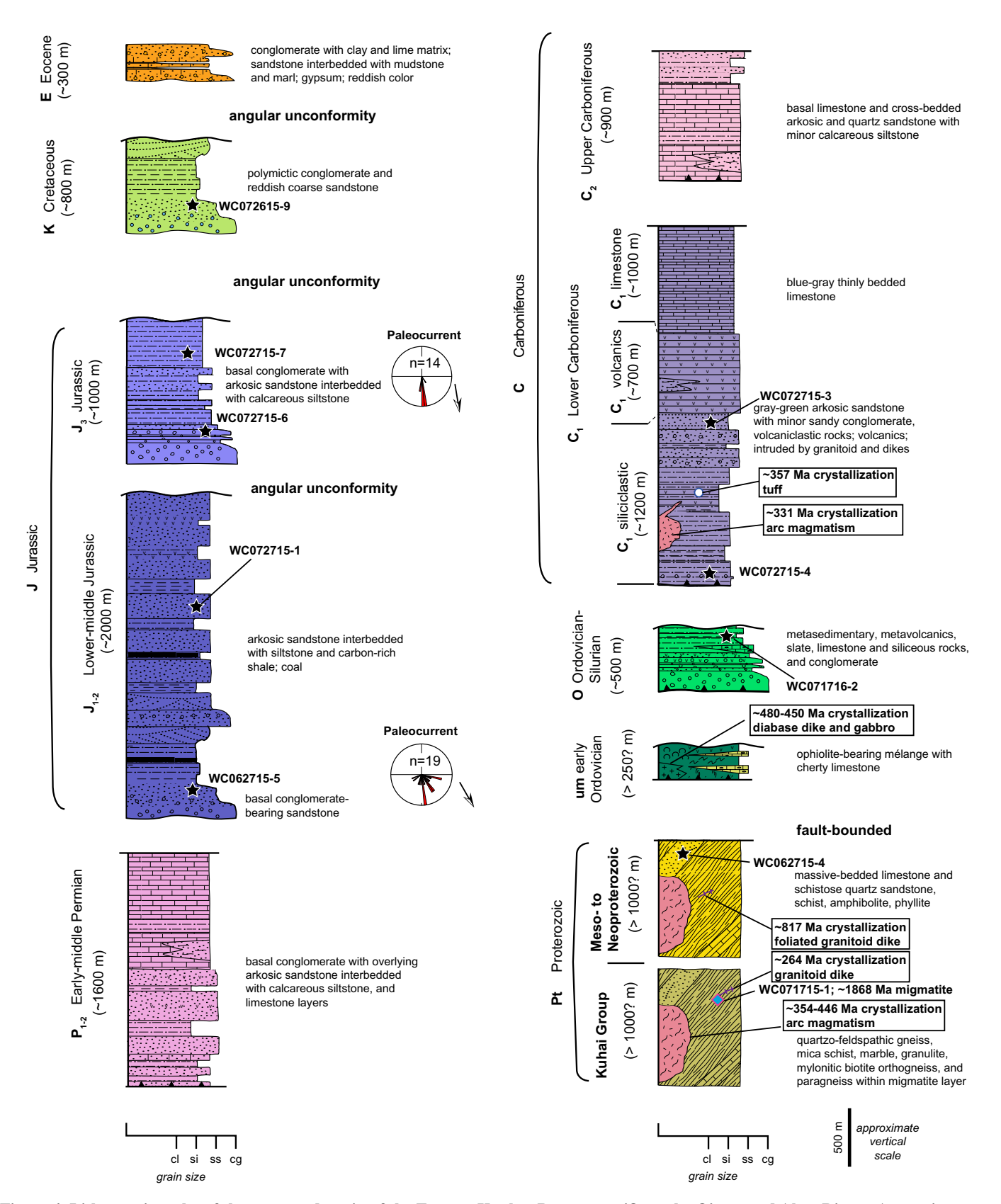


Figure 4. Lithostratigraphy of the western domain of the Eastern Kunlun Range, specific to the Qiemo and Aksu Rivers. Age assignments are from Xinjiang BGMR (1993), Xinjiang BGMR (2003), Pan et al. (2004), and our own observations. Also shown are U-Pb detrital zircon samples of major units (black stars; see Figs. 3 and 5) and geochronology results from Figure 7. Grain-size abbreviations: cl—clay; si—silt; ss—sandstone; cg—conglomerate.

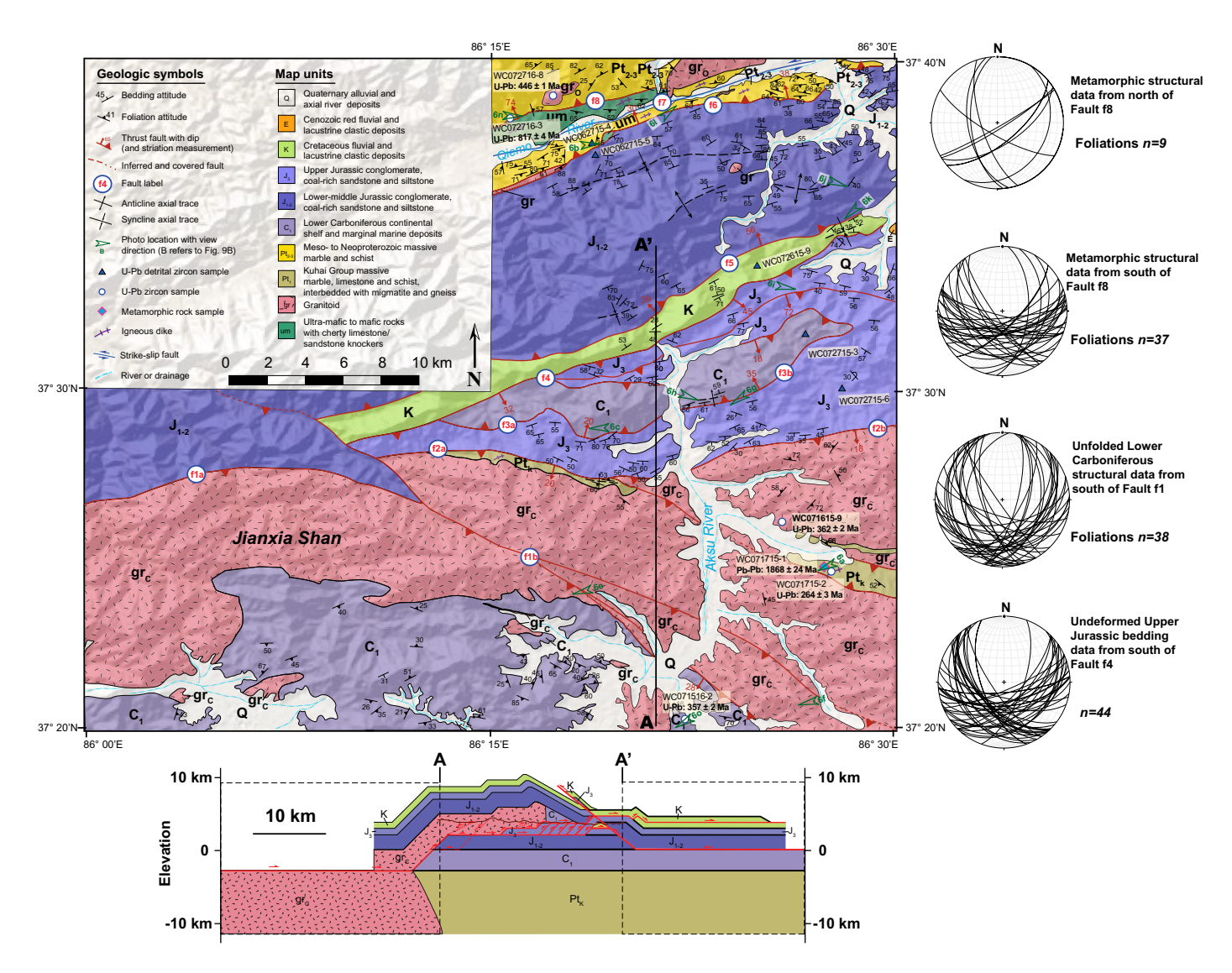


Figure 5. Top: Geologic map of a region in the northwestern domain of the Eastern Kunlun Range produced for this study. Underlying base map is from www.gscloud.cn. Bottom: Cross-section A-A', where the brown line is the topographic line, and the dashed boxes are the possible interpretation for the extension of the section A-A'.

of Pan et al. (2004) gave this unit a Changchengian age (i.e., Mesoproterozoic) on the basis of the regional geologic survey (Xinjiang BGMR, 2003). Foliated early Paleozoic granitoid rocks intrude both the gneiss and schist units. The foliations within in all of the metamorphic units are parallel across lithologic contacts, and all units are variably mylonitized (Fig. 6B). All of these metamorphic rocks are inferred to have Precambrian protolith ages (Xinjiang BGMR, 1993; Gehrels et al., 2003a; Pan et al., 2004), which is verified by our new geochronology data, discussed later herein.

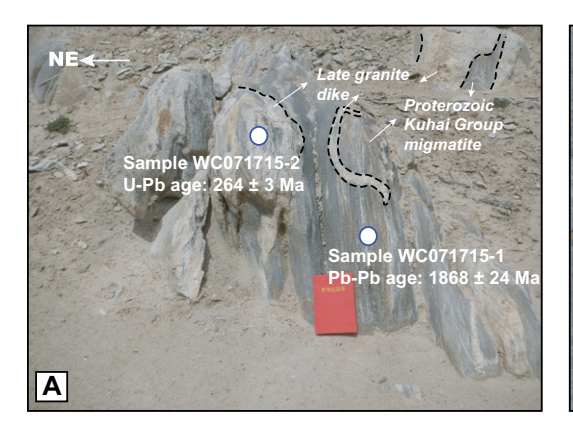
The Ordovician–Silurian Qimen Tagh Group (labeled O) consists of low-grade metamorphosed sandstone, siltstone, conglomerate, and slate with minor carbonate rocks, with volcanic rocks in the uppermost section. Although the

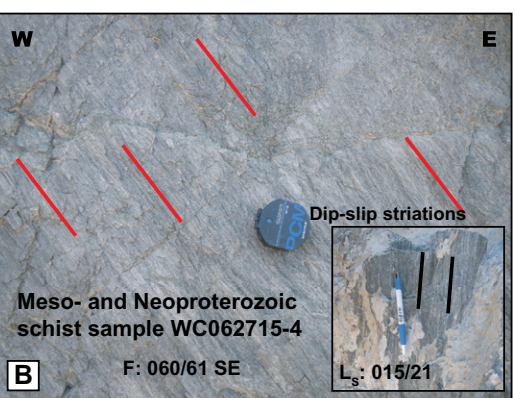
chronostratigraphy has been long debated, evidence from paleontology and zircon chronology suggests that the lower sandy slate section of this group is Lower Ordovician, and the uppermost volcanic section has yielded an age ca. 428 Ma (e.g., Qi et al., 2014). All Ordovician-Silurian rocks are strongly deformed, and the original sedimentary relationships are obscured. Devonian strata are absent from the study area, but they are found elsewhere in the western section of the Eastern Kunlun Range (e.g., C. Wu et al., 2016a; Yu et al., 2017). The rocks unconformably overlie the Ordovician-Silurian Qimen Tagh Group and are covered by biogenic carbonate rocks, which are often isoclinally folded, with transposed bedding (Pan et al., 2004; Xi et al., 2010).

Carboniferous strata are mainly divided into the lower Tuokuzidaban Group (labeled C_1) and

upper Halamilanhe Group (labeled C_2). The Lower Carboniferous rocks have a basal unit of massive, cross-bedded, gray-green arkosic sandstone with minor sandy conglomerate overlain by volcanic layers (Fig. 6C) and carbonate rocks. The Upper Carboniferous rocks are dominated by basal limestone and cross-bedded arkosic and quartz sandstone with minor calcareous siltstone. Conformably overlying these rocks, there are Lower Permian strata, which have a basal conglomerate and overlying arkosic sandstone interbedded with calcareous siltstone, and limestone layers.

Jurassic strata overlie the Lower Carboniferous rocks with a regional angular disconformity, and they are divided into the Lower-Middle Dameigou Formation (labeled J_{1-2}) and Upper Caishiling (labeled J_3) Formation. The





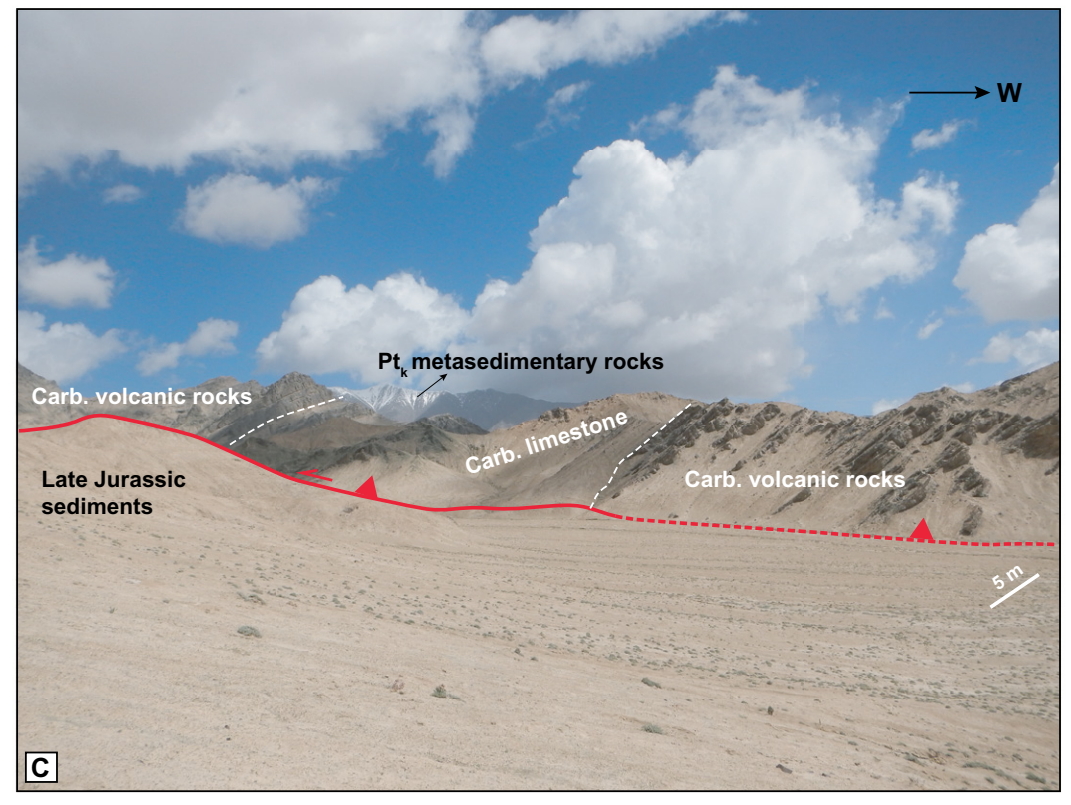


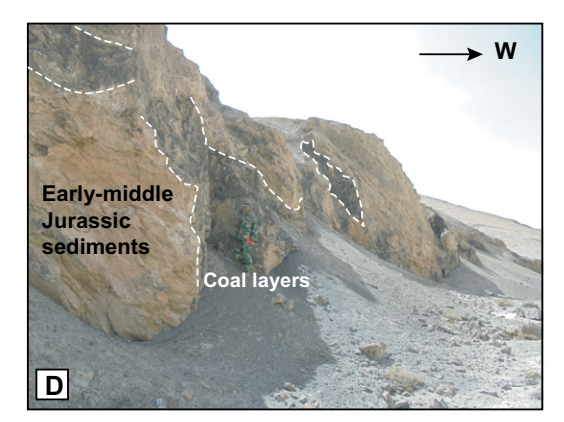
Figure 6 (on this and following page). Satellite and field photographs from the northwestern domain of the Eastern Kunlun Range displaying important geologic relationships discussed in text. Locations of photograph are shown in Figures 3 and 5. (A) A late granite dike intrudes into the Kuhai Group migmatite. (B) Mesoproterozoic and Neoproterozoic metamorphic rocks are placed over Lower-Middle Jurassic deposits; the photo shows an antithetic fault surface with steeply plunging fault striations and sample location. Photo was taken near fault f6 in Figure 5. (C) Carboniferous rocks are placed over Late Jurassic sediments; photo was taken at fault f3a in Figure 5.

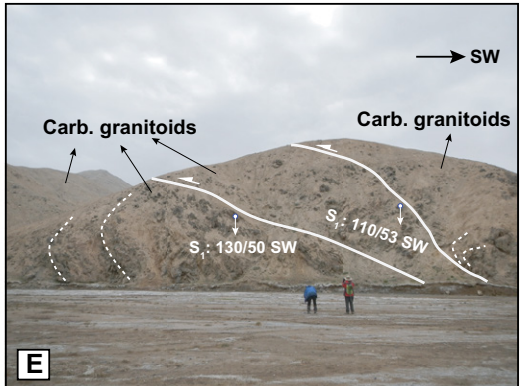
lower-middle unit consists of a basal conglomerate overlain by arkosic sandstone interbedded with siltstone, organic-rich shale, and numerous coal beds (Fig. 6D). Upper Jurassic rocks consist of a basal conglomerate with overlying arkosic sandstone interbedded with calcareous siltstone. Cretaceous rocks (labeled K) consist of polymictic conglomerate and coarse sandstone that is reddish in color. Cenozoic rocks are predominantly Lower Eocene in age (labeled E; Oinghai BGMR, 1991; Xinjiang BGMR, 2003). They consist of red fluvial and lacustrine sediments. Conglomerate, sandstone, and mudstone have a clay, marl, or limestone matrix. Quaternary sediments consist of alluvial, fluvial, and glaciofluvial deposits (Qinghai BGMR, 1991; Xinjiang BGMR, 2003).

Igneous Units

Numerous NE- to E-trending elongate early Paleozoic granitoid plutons are exposed throughout the Aksu and Qiemo River valley region, and most are attributed to arc and/or orogenic magmatism. These plutons have been assigned ages ranging from Early Cambrian—Ordovician to early Carboniferous (e.g., Xinjiang BGMR, 2003; Pan et al., 2004; this study), of which early Carboniferous magmatic activity is strongest in the south (Fig. 6E). Several large (up to ~200 km²) and some minor (1–10 km²) plutonic bodies are exposed as batholiths and stocks in the mapping area. They range in composition from calc-alkali low-K tholeiitic series to mafic to acidic rocks. These bodies

intrude the Proterozoic gneiss and schist and the early Paleozoic mélange, but they are thrust overlain by Lower Carboniferous and younger strata. Furthermore, these plutons intrude the contact between the Lower Carboniferous and Proterozoic basement units (Figs. 3 and 5), which requires that Carboniferous sediments were deposited on Proterozoic basement prior to intrusion. The units are mapped as undifferentiated granitoid (gr), except where a crystallization age has been determined, either from this study or other work. Our geochronology results presented later indicate that these plutons crystallized between ca. 446 and ca. 331 Ma. Minor dikes with compositions similar to the granitoids were also mapped and occurred within the migmatite in the mapping







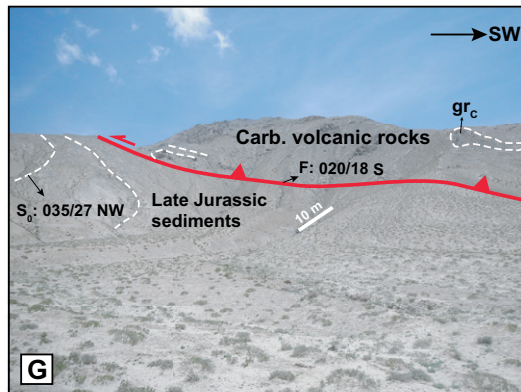
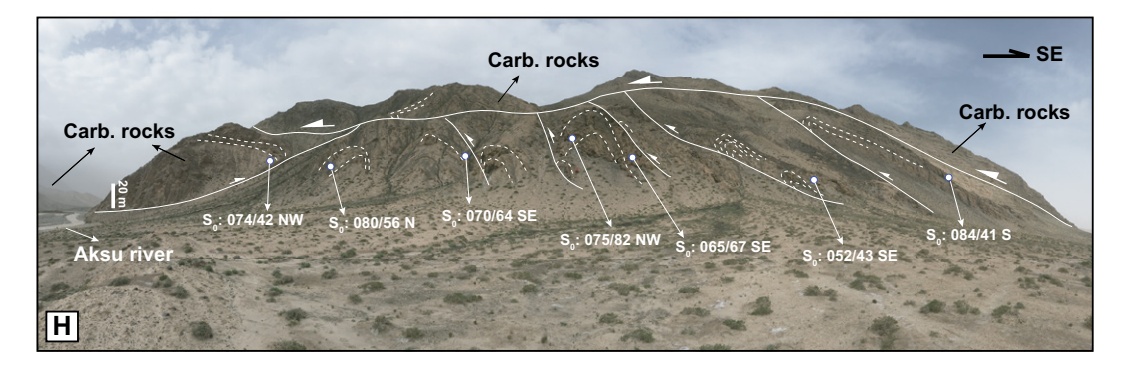


Figure 6 (Continued). (D) Early Jurassic sediments interbedded with coal layers. (E) Photo taken at fault f1a within the Carboniferous Jianxia Shan granitoid pluton in Figure 5. (F) View of south-verging hangingwall anticline in thrust fault f1a shown in Figure 5. (G) Carboniferous rocks are placed over Late Jurassic sediments; photo was taken at fault f3b in Figure 5. (H) Carboniferous rocks are placed over Jurassic sediments along the Aksu River.



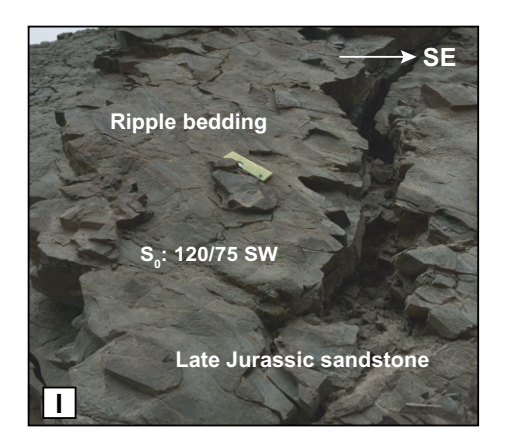
area. The late Paleozoic-early Mesozoic granitoids and dikes are scatted in the mapping area (Fig. 6A). Detailed geochronology and geochemistry analyses for Paleozoic-Mesozoic magmatism are in preparation and will be presented elsewhere.

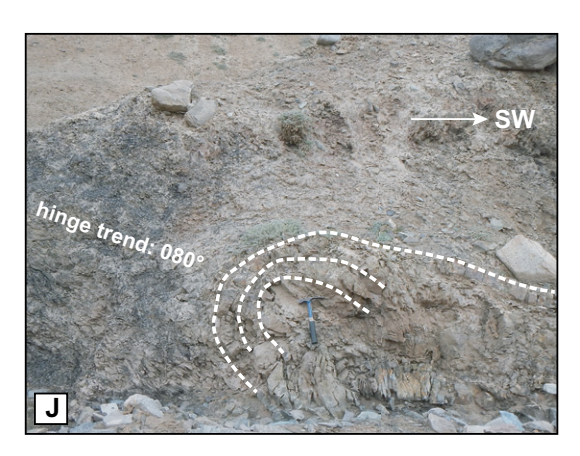
An ultramafic and mafic complex, locally referred to as the Munabulake ophiolite suite (Liu et al., 2009; Cao et al., 2013), is exposed in the northern portion of the mapping area. In the north flank of the Qiemo River, gabbroic plutonic rocks, diabase dikes, alkali feldspar granite, and basaltic volcanic rocks are found in Munabulake ophiolitic complex of the Southern Altyn mélange zone. This complex variably consists of ophiolitic mélange and fragments of an incipient oceanic arc and has been assigned an Ordovician

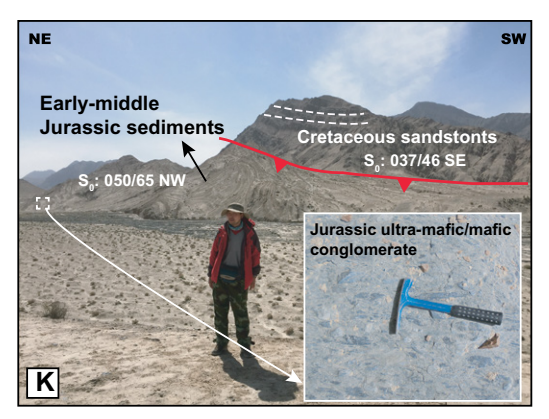
age based on reported geochronologic studies (Liu et al., 2009; Cao et al., 2013; this study). The unit consists of ultramafic to mafic rocks, basaltic andesite, gneiss, foliated granodiorite, marble, and limestone, and quartzite-sandstone knockers. In addition, there are outcrops of massive plagioclase-pyroxene gabbro. There is significant deformation within the complex, and the lithologic contacts are highly sheared (Fig. 5). Taken together, this unit represents part of the Southern Altyn Tagh suture zone, which connects with the Mangnai ophiolite to the southeast. The complex units are only juxtaposed against the Mesoproterozoic and Neoproterozoic marble unit, and, where observed, the Mesoproterozoic and Neoproterozoic unit is always structurally beneath the ophiolite suite (Fig. 5).

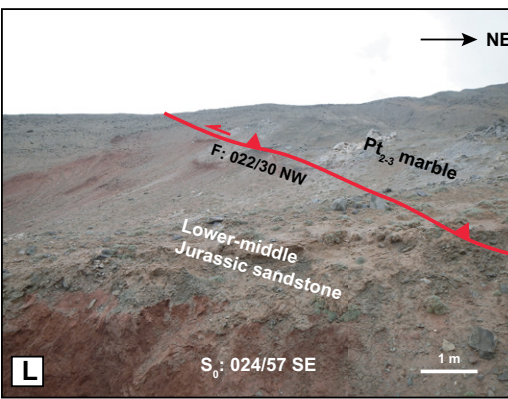
Although this tectonic contact may have been reactivated in the Cenozoic, this relationship suggests that the Mesoproterozoic and Neoproterozoic strata were originally thrust beneath the obducted ophiolite suite during the South Altyn Tagh orogeny.

As discussed above, foliated granitoid dikes (granodiorite to quartz diorite) intrude Proterozoic metamorphic rocks. This unit is variably mylonitized with well-defined stretching lineations, and in certain locations both quartz and feldspar grains appear to have deformed ductilely and recrystallized. Our geochronology results indicate that this foliated granitoid has crystallization ages of ca. 817 Ma. This age provides a minimum-age bound for the protolith of the metamorphic complex into which it intrudes.









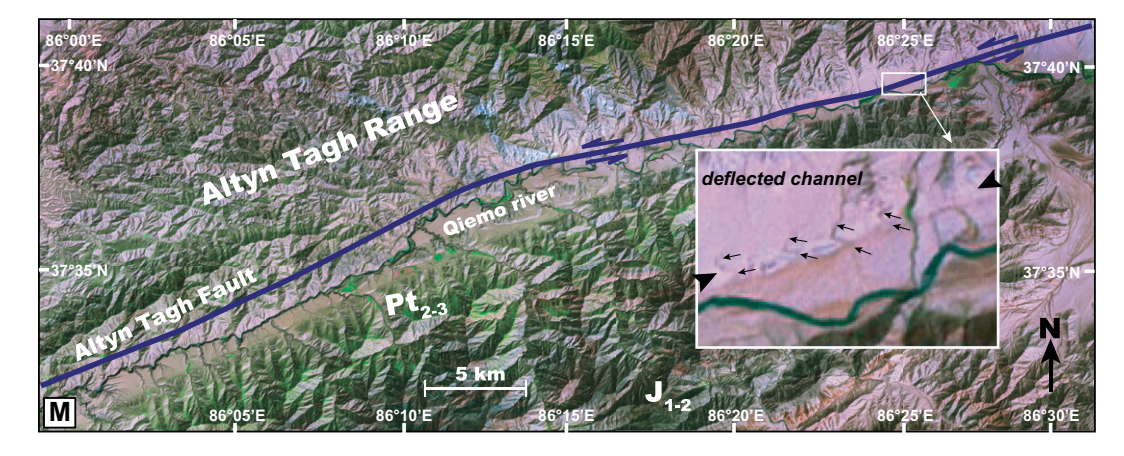


Figure 6 (Continued). (I) Ripple bedding structure on the Late Jurassic sandstone. (J) View of north-verging hanging-wall anticline near thrust fault f5 shown in Figure 5. (K) Early-Middle Jurassic rocks placed over Cretaceous sediments; photo was taken at fault f5 in Figure 5. Inset shows the Jurassic ultramafic/mafic conglomerate. (L) Mesoproterozoic and Neoproterozoic metamorphic rocks are placed over Lower-Middle Jurassic deposits; photo was taken at fault f6 in Figure 5. (M) High-resolution satellite image showing the active left-slip Altyn Tagh fault with blue line along the Qiemo River (see Fig. 3). Inset shows deflection of a through-going channel (arrowed) at 86°25'E (e.g., Cowgill, 2007).

Regional Unconformities

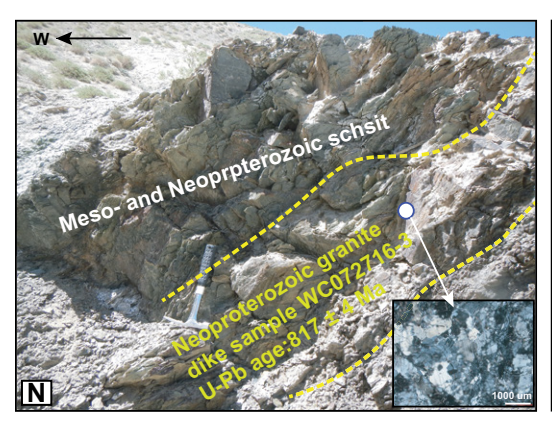
Three distinct Phanerozoic unconformities are recognized in the mapping area, and they are named for the unit that overlies the unconformity. The oldest unconformity, which is also the most widespread, consists of Jurassic strata overlying Proterozoic basement (e.g., Kuhai Group along the Aksu River; Mesoproterozoic to Neoproterozoic rocks along the south bank of the Cherchen River) and Ordovician—Silurian strata (i.e., Qimen Tagh Group). This requires the Proterozoic basement and Ordovician rocks to have been at or near the surface at the time of

Jurassic deposition. This unconformity is a key marker horizon in the balanced cross-section restorations.

The Mesozoic unconformities, with a variety of angular unconformities at the base of Jurassic and Cretaceous rocks, were caused by regionally extensive tectonic events across northern Tibet (e.g., Vincent and Allen, 1999; Chen et al., 2003). In one locality along the southern bank of the Cherchen River, Cretaceous rocks unconformably overlie Carboniferous and Jurassic rocks. This observation provides two important constraints. First, the Carboniferous and Jurassic rocks were both at or near the surface at the

time of Cretaceous deposition. Second, an event is required to have tilted the Jurassic unconformity and Carboniferous—Permian rocks prior to the deposition in the Cretaceous.

Cenozoic rocks, assigned a Paleocene to early Eocene age, are only exposed in the eastern portions of the mapping areas (Figs. 3 and 5). They were deposited on top of Cretaceous and Lower Jurassic strata, which indicates that prior to Cenozoic deformation, these Mesozoic rocks were closest to the surface. The development of this unconformity represents the initiation of Cenozoic deformation related to the Tibetan orogen. Further interpretation of the depositional setting



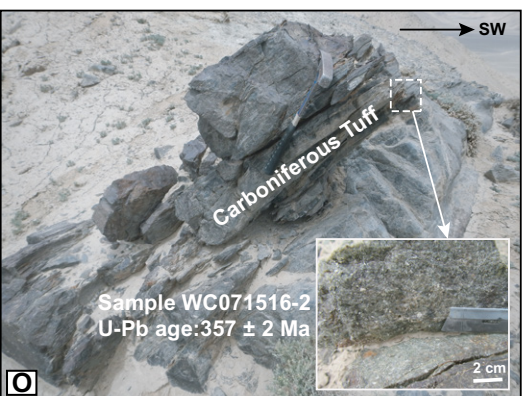


Figure 6 (Continued). (N) Neoproterozoic granite dike intrudes into the Mesoproterozoic and Neoproterozoic schist. (O) Photo and inset showing the tuff sample within the Lower Carboniferous Tuokuzidaban Formation.

of these Cenozoic rocks is not within the scope of this study.

Structural Geology

Structures dominantly trend NE, including the strike of sedimentary units, strike of foliations within the metamorphic units, trend of the ranges, and surface traces of major faults. Deformation can be categorized into three distinct regimes: (1) left-lateral shearing and faulting associated with the Altyn Tagh fault, (2) Cenozoic dip-slip contractional structures, including thrust faults and folds, and (3) early Paleozoic faulting, ductile shearing, and metamorphism. There is no direct evidence of Mesozoic deformation or normal faulting, but our field observations are consistent with earlier work that suggests that Jurassic and Cretaceous sedimentation was caused by regional extension (Vincent and Allen, 1999; Chen et al., 2003; Yin et al., 2008b; Zuza et al., 2019), including fining-upward sequences and growth strata relationships.

We interpret deformation of Carboniferous and younger strata to be Cenozoic in age based on the following observations: (1) Most observed faults and folds of Lower Carboniferous and younger rocks merge with active rangebounding thrust faults; (2) these faults truncate Cenozoic terrestrial deposits and Quaternary alluvium; and (3) Jurassic and Cretaceous strata were probably extension related (e.g., Vincent and Allen, 1999; Chen et al., 2003; Yin et al., 2008a, 2008b; Zuza et al., 2019), so contractional structures involving these rocks must be Cenozoic in age. This also implies that folding and duplication of the Jurassic unconformity occurred in the Cenozoic.

Next, we present a detailed structural analysis of each river valley, including juxtaposition geometries, map-view relationships, kinematic indicators, and alternative interpretations, starting with the north flank of the Aksu River valley in the south and progressing to the north (Fig. 3). The NE- to E-striking thrust faults are labeled

f1 through f8, from south to north, respectively (Fig. 5), and are discussed in this order below.

Fault f1

The WNW-striking fault dips 28° to the NE, juxtaposes early Carboniferous granitoids (Fig. 6E) against Lower Carboniferous strata (C₁), and truncates overlying Jurassic sediments to the west (Fig. 5). In the west, this fault is labeled f1a, and it is a W-striking, S-dipping feature that places the hanging wall of early Carboniferous granitoids over Lower-Middle Jurassic strata (J_{1-2}) . Fault 1a must be relatively low angle (~20°S) based on its map trace. This fault merges to the east with fault f1b. In the east, f1b branches into several fault splays, which variably place early Carboniferous granitoids and Lower Carboniferous strata over other granitoids. Fault f1b cuts the granitoid and overlying shallow-marine, lacustrine, and continental shelf sedimentary strata, but offset diminishes within the folded granitoid (Fig. 6F). The foliation data from the Carboniferous rocks were compiled and analyzed in several stereonets (Fig. 5) using Stereonet 9 (software by Rick Allmendinger). In the south of f1, the foliations are variable, generally striking NW (Fig. 5).

Fault f2

This W-striking, S-dipping thrust fault (thrust dipping 18°S-20°S) places Proterozoic metamorphic basement (Pt_v) and early Carboniferous granitoids (gr) over Upper Jurassic strata (J₃). Here, we denote the western and eastern traces of these faults as f2a and f2b, respectively. Fault 2a places Proterozoic Kuhai Group metamorphic rocks over Late Jurassic Caishiling Formation sediments, and a minor (~150-m-wavelength) hanging-wall anticline forms in the hanging wall of this thrust fault. This fault is truncated to the east by f1b. At the eastern portion, f2a branches into several fault splays, which variably place Proterozoic (Pt_K) rocks over Jurassic sediments and early Carboniferous granitoids. Fault f2b places early Carboniferous granitoids thrust over Late Jurassic sediments, and it is relatively low angle (~18°S) based on its map trace. Upper Jurassic strata in the footwall of f2 are internally deformed, with numerous 100-m-wavelength folds and faults.

Fault f3

This thrust fault places early Carboniferous sediments as a klippe over Upper Jurassic strata. In the west, this fault is labeled as f3a, and it merges to the west with f4. Where this fault is exposed in a minor footwall syncline of this thrust, the fault surface dips 20°N. At this locality, the Carboniferous strata in the hanging wall are parallel to the fault, and Jurassic rocks in the footwall are oblique to the fault surface (Fig. 6G). In the east, this fault is labeled as f3b. There is a prominent ~1-km-wide anticline in the hanging wall of f3b, and the fault surface dips 35°N. This fault is overturned in the north, and the fault surface dips 18°S. The fault trace to the west is obscured by Aksu River (Fig. 6H).

Fault f4

The NE-striking thrust fault dips 32-45°SE and places early Carboniferous strata (C1) and Late Jurassic strata (J₃) over Lower Cretaceous sediments (K). The fault trace of f4 to the east is covered by Quaternary sediments, but it is assumed that the fault is truncated to the west by f1b. Fault f4 branches into several fault splays, which variably juxtapose early Carboniferous and Late Jurassic strata over other Late Jurassic sediments, but the offset diminishes within the Late Jurassic sediments. Where observed, this splay fault surface dips 72°S within the Jurassic strata. The fault has a footwall syncline with <1 km wavelength in the east; at this locality, the hanging-wall Jurassic strata are overturned. Sedimentary marks, such as ripples, on the bedding surface of the Late Jurassic sandstones indicate the southward direction of the paleocurrent (Fig. 6I). In the Late Jurassic rocks to the south of f4, the bedding is roughly parallel and dips to south (Fig. 5).

Fault f5

The NE-striking thrust fault dips 39-56°NW, and the fault places an ~10-km-wide hangingwall anticline of Lower-Middle Jurassic strata (J_{1.2}; Fig. 6J) over a minor footwall syncline of Lower Cretaceous sediments (K; Fig. 6K). This fault appears to either be truncated by, or merge with, f1b in the west, although this relationship is not directly observed (Fig. 5). Map view relationships suggest that offset increases to the east, but exposure is obscured by Quaternary sediments (Fig. 6K). Ultramafic and mafic rocks are the major components of the conglomerate layer of the Lower-Middle Jurassic strata (Fig. 6K), which indicates that the Altyn Tagh Range to the north is the main possible provenance of these sediments.

Fault f6

The ENE-striking thrust fault f6 dips 30°-38° to the NW, and the fault places Mesoproterozoic to Neoproterozoic undifferentiated massive marble and schist with intrusions over footwall syncline of Lower-Middle Jurassic strata (J₁₋₂; Fig. 6L). This fault merges to the northeast with the Altyn Tagh fault (Fig. 3) and represents the southernmost termination structure of this major strike-slip fault, which strikes parallel to the Altyn Tagh fault (Fig. 1B). Although no direct fault kinematic measurements were made for this fault, the fold axes are parallel to the fault strike, which may suggest that this fault is primarily a dip-slip structure (Fig. 6B). Fault offset must be <1 km based on the map-view relationships, and the tight (~1-km-wavelength) hanging-wall folds accommodate a similar magnitude of shortening. The fault is covered by Quaternary river deposits in the northeast, and its western extent is unknown. The fault strike is parallel to the nearly E-W-trending Qiemo River (Fig. 5).

Fault f7

The active, left-slip Altyn Tagh fault was not observed in the field along the southern Cherchen River, but the morphologic expression of the fault trace is very distinct for much of its length. The fault trace crosses the extreme western end of Tula Basin (Fig. 2) and has clearly disrupted Quaternary alluvial deposits (Fig. 6M). No offset geologic markers associated with this fault from which slip magnitude may be estimated were evident in the outcrops of the mapping area. Rather, left-slip displacement, which appears to be best characterized at the Cherchen River site (~86.4°E), yielded a revised slip rate of 9.4 ± 2.3 mm/yr (Fig. 6M; Cowgill, 2007), consistent with data from the Sulamu Tagh site (~87.4°E) ~20 km to the east (Mériaux et al., 2005).

Fault f8

The ENE-striking thrust fault f8 dips 74° to the NW and places Mesoproterozoic to Neoproterozoic metamorphic rocks against the ultramafic and mafic complex. The ultramafic and mafic complex in the footwall of f7 is internally strongly deformed and sheared, with numerous 100-m-wavelngth folds and faults, and the timing of their activity is unconstrained in this study. Fault f7 is covered by an early Paleozoic pluton in the east but crosscuts the Neoproterozoic igneous dikes (Fig. 6N). Although this tectonic contact may have been reactivated in the Cenozoic, this relationship suggests that the fault contact may originally been from the early Paleozoic. The Proterozoic schist unit has strongly developed foliations and minor stretching lineations. These fabrics are inferred to have developed in the early Paleozoic as a result of the Altyn Tagh arc and subsequent orogeny. Our new geochronologic analyses suggest that this broad shear zone was active in the Early Ordovician, and ductile shearing ceased by ca. 446 Ma, when the foliated metamorphic rocks were crosscut by an undeformed granitoid with a U-Pb age of 446 ± 1 Ma (i.e., sample WC072716-8). The foliation data from the Mesoproterozoic and Neoproterozoic metamorphic rocks were compiled and analyzed in several stereonets (Fig. 5) using Stereonet 9. In the metamorphic rocks to the north of f8, the foliations are roughly parallel, near vertical, and strike NW. South of f8, the data are more diverse, and the foliations are variable, generally NE striking (Fig. 5). The rocks to the north of the Altyn Tagh match or correlate with features such as the Qilian arc (Wu et al., 2016a, 2017; Zuza et al., 2018).

METHODS

Sandstone Petrography

We used a cross-polarization microscope to observe the petrographic features, including mineral composition, grain size, sorting, and roundness. Modal compositions were then determined utilizing the modified Gazzi-Dickinson point-counting method (Ingersoll et al., 1984). A minimum of 370 points were counted per sample. Raw point-counting data are summarized in the supplementary material. Samples were classified and plotted on the ternary diagrams using the scheme outlined in Dickinson et al. (1983).

We followed the mineral abbreviation of Dickinson and Suczek (1979) to better describe our results: Qt for total quartz, Qm for monocrystalline quartz, F for feldspar, L for lithic rock fragments, and Lt for total lithic grains, including polycrystalline quartz. Detailed data for these five sandstones are shown in the supplementary material Table DR1 (see footnote 1).

U-Pb Zircon Geochronology

Zircon grains for U-Pb dating were separated from 9 sandstones, 5 igneous rock samples, and 1 metamorphic rock sample by traditional methods and mounted in epoxy with standard zircons. Individual zircon grains were picked by hand under a binocular microscope. Zircons of each sample were randomly selected, mounted in epoxy resin, and polished, in order to conduct U-Pb dating. Most zircons were analyzed using an Agilent 7500a inductively coupled plasma-mass spectrometer (ICP-MS) coupled with a New Wave Research UP193FX excimer laser at the Key Laboratory of Continental Collision and Plateau Uplift, Institute of Tibetan Plateau Research, Chinese Academy of Sciences, Beijing. The laser-ablation (LA) multicollector (MC) ICP-MS analytical methods were described in Gehrels et al. (2011) and are briefly summarized here. The measurements were made on a Micromass Isoprobe using Faraday detectors for ²³⁸U, ²³²Th, and ²⁰⁸Pb-²⁰⁶Pb and an ion-counting channel for 204Pb on the LA-MC-ICP-MS. Common Pb corrections were made using the measured 204Pb and assuming an initial Pb composition from Stacey and Kramers (1975). The primary standard used was GJ1 (Jackson et al., 2004). The secondary standards were 91500 (²³⁸U/²⁰⁶Pb age of 1065 Ma), and Plesovice (238U/206Pb age of 337 Ma).

Ages presented are ²⁰⁶Pb*/²³⁸U ages for grains younger than ca. 1000 Ma and ²⁰⁶Pb*/²⁰⁷Pb* ages for grains older than ca. 1000 Ma. To interpret the crystallization ages for the igneous samples, we only examined zircon analyses with discordance of <10%. We focused on the dominant population of younger analyses, and we interpreted the weighted mean age of the youngest cluster $(n \ge 3)$ of zircon ages as the crystallization age (Table 1). Anomalously younger zircon ages probably were the result of Pb loss due to a younger metamorphic event, and older zircon grains were interpreted as inherited grains. Uncertainties on individual analyses are given at the 1σ level and plotted as the 2σ level. All uncertainties, including analytical and systematic, of the weighted mean ages are reported at the 95% confidence level. The weighted mean ages and probability density distributions were calculated and plotted using Isoplot 3.0 of Ludwig (2003). For the detrital zircon age data, we only

¹GSA Data Repository item 2019388, including Jurassic sandstone petrography raw point-counting data, and zircon U-Pb isotopic data for the igneous, metamorphic, and detrital samples, is available at http://www.geosociety.org/datarepository/2019 or by request to editing@geosociety.org.

TABLE 1. SUMMARY OF ZIRCON GEOCHRONOLOGY RESULTS

Sample	Rock type	Latitude (°N)	Longitude (°E)	Interpreted age (Ma)	MSWD	n
Igneous and metamorphic samples				Crystallization age		
WC071516-2	Tuff	37°20.123′	86°23.768′	357 ± 2	1.15	16 out of 38
WC072716-3	Foliated granitic dike	37°38.873′	86°15.623′	817 ± 4	2.4	16 out of 62
WC072716-8	Granodiorite	37°39.136′	86°17.028′	446 ± 1	4.1	28 out of 41
WC071615-9	Granite	37°27.276′	86°25.017′	362 ± 2	0.18	26 out of 30
WC071715-2	Granite	37°25.067′	86°27.925′	264 ± 3	3.5	8 out of 19
WC071715-1	Migmatite	37°25.067′	86°27.925′	1868 ± 24	3.5	3 out of 42
Sedimentary and metasedimentary samples				Maximum depositional age		
WC062715-4	Foliated quartz schist	37°38.172′	86°18.316′	1014 ± 18	0.53	3 out of 97
WC071716-2	Quartz schist	37°42.929′	86°51.374′	507 ± 16	4.1	3 out of 89
WC072715-4	Quartzite	37°28.522′	86°43.579′	400 ± 12	7	3 out of 98
WC072715-3	Sandstone	37°32.588′	86°26.987′	359 ± 8	7	3 out of 50
WC062715-5	Coarse-grained sandstone	37°37.916′	86°37.916′	242 ± 28	1.29	3 out of 100
WC072715-1	Fine-grained sandstone	37°37.499′	86°32.688′	227 ± 7	4.9	3 out of 85
WC072715-6	Medium-grained sandstone	37°30.622′	86°28.837′	193 ± 1	0.33	3 out of 83
WC072715-7	Pink-brown sandstone	37°15.176′	86°43.923′	156 ± 2	0.51	3 out of 96
WC072615-9	Sandstone	37°34.869′	86°24.622′	124 ± 10	0.66	3 out of 59

Note: MSWD—mean square of weighted deviates.

considered analyses that were <30% discordant or <5% reversely discordant (Table 1; e.g., Gehrels et al., 2011). Normalized probability density plots were used to compare the different data sets using 2010 software provided by the Arizona LaserChron Center. The geochronologic data are provided in Table DR2 (see footnote 1).

SAMPLE DESCRIPTIONS AND RESULTS

Igneous and Metamorphic Zircon Geochronology Results

Tuff sample WC071516-2 was collected on the volcanic tuff layer interbedded within the Lower Carboniferous Tuokuzidaban Group (C_1 ; Figs. 6O and 7A). Thirty-eight zircons were analyzed, and U-Pb ages ranged from 343 Ma to 666 Ma (Fig. 8A). The weighted average of 16 concordant analyses was 357 ± 2 Ma (mean square of weighted deviates [MSWD] = 1.15), which we interpret as the crystallization age of the tuff (Table 1). The other analyses were excluded because of discordance or low radiogenic Pb. The zircons with these ages might have originated from the source region of the magmatic rocks, or they may have been incorporated from country rocks during magma eruption.

Neoproterozoic foliated granitic dike sample WC072716-3 was collected from a foliated granitic dike that intrudes into the medium- to low-grade metamorphosed unit (Pt_{2-3}) located in the hanging wall of the fault f7 (Figs. 6N and 7B). Analyses of zircon grains from sample WC072716-3 yielded 62 concordant yet diverse ages, ranging from a U-Pb age of 752 Ma to 983 Ma (Fig. 8B). The older population of 13 grains yielded a weighted mean age of 888 ± 5 Ma (MSWD = 2.1), which is interpreted to be inherited. The younger population of 16 analyses yielded a weighted mean age of 817 ± 4 Ma (MSWD = 2.4), which is interpreted

as the crystallization age of this Neoproterozoic granite (Table 1).

Early Paleozoic granodiorite sample WC072716-8 is part of a slightly foliated granite sill located along the northwestern flank of the Qiemo River (Figs. 5 and 7C). Forty-one grains were analyzed, and all yielded concordant ages ranging from 378 Ma to 1265 Ma (Fig. 8C). One single age was distinctly younger (ca. 378 Ma), which may have resulted from Pb loss during a younger metamorphic event, and one population of ages was distinctly older, possibly due to older zircon-grain inheritance. The weighted mean of the average population of 28 ages is 446 ± 1 Ma (MSWD = 4.1), which we interpret as the best estimate of a crystallization age (Table 1).

Lower Carboniferous granite porphyry sample WC071615-9 is part of Jianxia Shan pluton located along the eastern flank of the Aksu River (Figs. 5 and 7D), which intrudes into the Proterozoic Kuhai Group medium- to high-grade metamorphic rocks (PtK). Thirty grains were analyzed, and all yielded concordant ages ranging from 358 Ma to 2033Ma (Fig. 8D). The weighted mean of the average population of 26 ages was 362 ± 2 Ma (MSWD = 0.18), which we interpret as the best crystallization age of the Lower Carboniferous-latest Late Devonian granitoid pluton (Table 1). One single early Paleozoic age is distinctly older (ca. 459 Ma), possibly due to older zircon-grain inheritance (Fig. 8D). In addition, a Paleoproterozoic inherited zircon core age of ca. 2033 Ma also occurred in this granite sample (Fig. 8D), which is possible related to the metamorphic basement of the western domain of the Eastern Kunlun Range.

Undeformed late Paleozoic granite dike sample WC071715-2 was collected from a granite dike that intrudes the internally deformed migmatite (Figs. 6A and 7E). Nineteen zircons were analyzed, and U-Pb ages ranged from 221 Ma to 322 Ma (Fig. 8E). The weighted average of eight concordant analyses was 264 ± 3 Ma

(MSWD = 3.5; Table 1). The other analyses were excluded because of discordance or low radiogenic Pb.

Migmatite sample WC071715-1 was collected from the migmatite layer of the Kuhai Group (Figs. 6A and 7F). Analyses of zircon grains from sample WC071715-1 yielded 52 concordant yet diverse ages, ranging from a U-Pb age of 260 Ma to a Pb-Pb age of ca. 2435 Ma (Fig. 8F). Several distinct age populations were observed, and there was significant zircon inheritance. The cathodoluminescence-dark rims with oscillatory zoning showed much higher U and lower Th/U (usually 0.02-0.61; Table DR2) and were strongly discordant (207Pb/206Pb ca. 1.0-2.4 Ga; Fig. 8F). When all data are plotted on a concordia diagram, they align in a discordia with an upper intercept at 1907 \pm 40 Ma and lower intercept at 680 ± 110 Ma (Fig. 8F). However, it is evident that some of the most discordant data points (all with very high U contents) are slightly off the discordia and closer to the concordia (Fig. 8F), which suggests that they may be younger. No clear regional signals of the lower-intercept Neoproterozoic overprint are shown by the zircons from this sample. Furthermore, a single inherited core has a 207Pb/206Pb age of 2435 ± 8 Ma, and this is the oldest zircon found in this sample. The age population near the upper intercept is concordant and yielded a weighted mean 207 Pb/ 206 Pb age of 1868 ± 24 Ma (MSWD = 3.5; Fig. 8F), which is taken as the best estimate of the magmatic crystallization age of this sample (Table 1). Alternatively, these other young ages may reflect later pulsed intrusion or slow cooling.

Sandstone Petrographic Results

In order to ascertain the tectonic settings of the sedimentary units from which our samples were collected, we performed sandstone composition analysis for the Jurassic samples (Fig. 9).

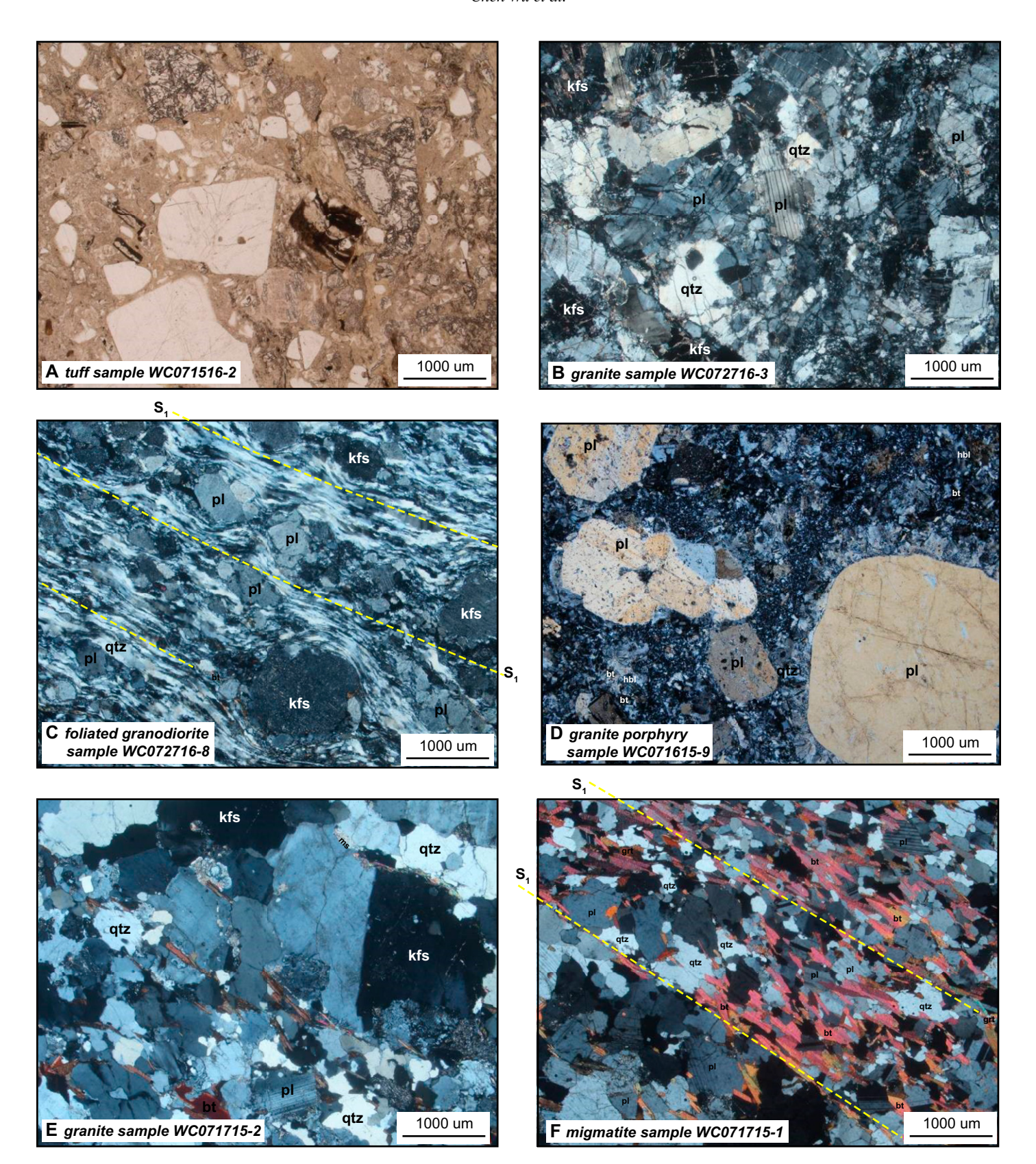


Figure 7. Photomicrographs of the igneous and metamorphic samples in this study. Abbreviations for minerals: qtz—quartz; pl—plagio-clase; bt—biotite; kfs—K-feldspar; ms—muscovite; hbl—hornblende; grt—garnet. All photomicrographs were taken under cross-polarized light.

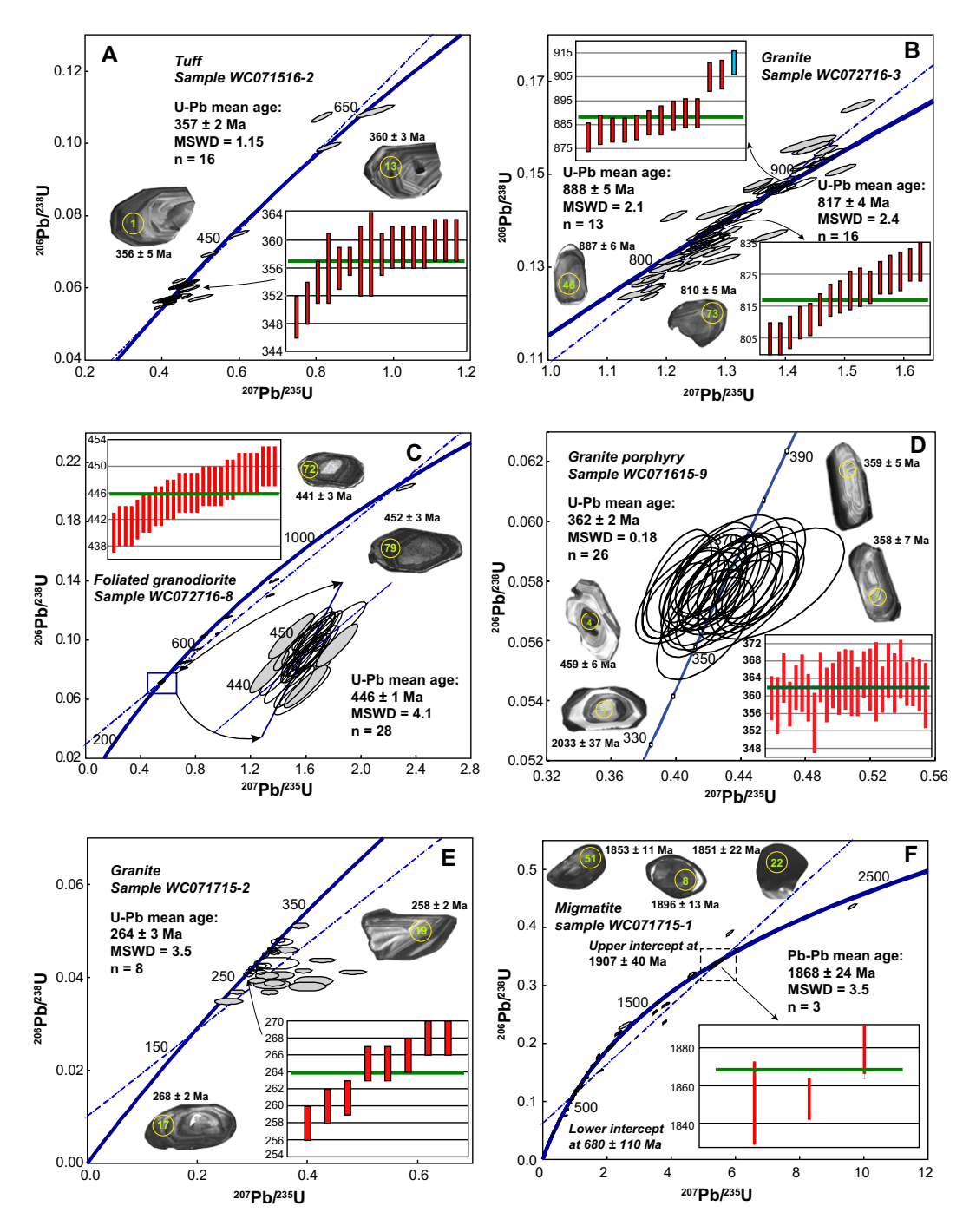


Figure 8. U-Pb concordia diagrams showing results of single shot zircon analyses and relative probability plots of zircon ages for each sample. Error ellipses are 25, and gray shaded ellipses show individual analyses that were excluded from weighted mean calculations. Only concordant ages are plotted in probability distributions, and crossed out peaks were not included in weighted mean calculation. All weighted mean ages are U-Pb ages (unless specified) at the 95% confidence level. See text for further discussion of rationale and Figures 3 and 5 for sample locations. Plots were created with Isoplot 4.1 of Ludwig (2003). See Table DR2 (see text footnote 1) for detailed data set. MSWD-mean square of weighted deviates.

The reason we did not conduct sandstone composition analysis on other samples was due to the effects of metamorphism and grain size. Specifically, the grain size of the Lower Cretaceous sample was too fine (<0.0625 mm) to be appropriate for sandstone composition analysis (Dickinson, 1970, 1985). Carboniferous, Ordovician, and Proterozoic samples are metamorphosed sandstones, with grain recrystallization and the development of cleavage schistosity.

Sample WC062715-5 was collected from a gray-brown, coarse-grained sandstone that lies

at the base of a sequence of interbedded sandy conglomerate, conglomerate-bearing coarse sandstone, and carbon-rich shale. The sequence is the lower part of the Lower–Middle Jurassic Dameigou Formation exposed locally along the southern bank of the Qiemo River. Detrital modes were found to be: Qt:F:L = 65:21:14 and Qm:F:Lt = 62:21:17 (Table DR1). Sample WC072715-1 was collected from a gray-green, medium- to fine-grained sandstone that lies at the base of a sequence of interbedded fine-grained sandstone, siltstone, and carbon-rich shale. This

sequence is the upper section of the Lower–Middle Jurassic Dameigou Formation exposed locally along the southern bank of the Cherchen River. Detrital modes are Qt:F:L = 55:21:24 and Qm:F:Lt = 49:21:30 (Table DR1). These sandstones are moderately well sorted with rounded to subrounded framework grains, calcite cement, and secondary hematite. Monocrystalline quartz is the secondary component, while polycrystalline quartz is rare. The quartz grains are commonly subrounded to rounded. Zircon, muscovite, and magnetite are common accessory

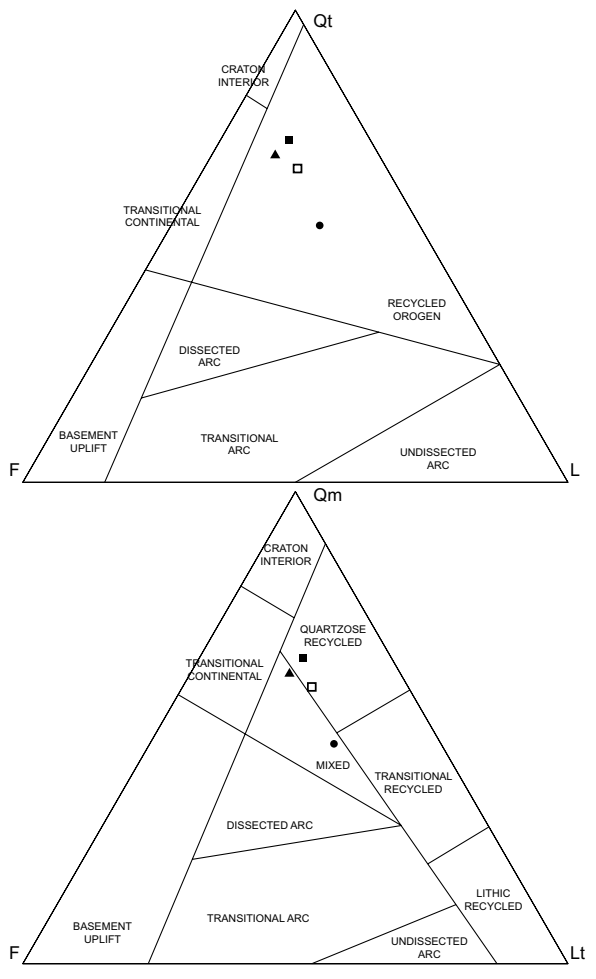


Figure 9. Ternary diagrams (QtFL and QmFLt) indicating modal abundances recalculated from raw point-counting data (Table DR1; see text footnote 1) for sandstone samples. The provenance fields of Dickinson et al. (1983) are shown to aid in potential source interpretation. Qt—total quartz, Qm—monocrystalline quartz, F—feldspar, L—lithic rock fragments, Lt—total lithic grains, including polycrystalline quartz.

Lower-middle Jurassic: ▲ Sample WC062715-5 ◆ Sample WC072715-1

Upper Jurassic: ■ Sample WC072715-6 □ Sample WC072715-7

minerals. Results for both samples plot in the "recycled orogen" field in the QtFL diagram featuring recycled source areas, and in the "mixed" field in the QmFLt diagram (Fig. 9).

Sample WC072715-6 was collected from a red-brown, medium-grained sandstone that lies at the base of a sequence of interbedded sandy conglomerate, argillaceous siltstone, and finegrained sandstone. The sequence is part of the Upper Jurassic Caishiling Formation exposed locally between faults f2b and f3b along the eastern bank of the Aksu River. Sample WC072715-7 was collected from a pink-brown, medium-grained sandstone that locally exposed the upper layer of the regional unconformity at the base of the Upper Jurassic strata, which unconformably overlie Paleoproterozoic Kuhai Group metasedimentary rocks. These sandstones are mostly poorly sorted, include siliceous or calcareous cements, and feature angular to subrounded grains. Detrital modes of sample WC072715-6 are Qt:F:L = 70:17:13 and Qm:F:Lt = 64:17:19, whereas the modal compositions for sample WC072715-7 are

Qt:F:L = 62:19:19 and Qm:F:Lt = 59:19:22 (Table DR1). These modal abundances of Caishiling Formation sandstones plot in the "recycled orogen" and "quartzose recycled" fields on the ternary diagrams, featuring recycled source areas (Fig. 9).

Detrital Zircon Geochronology Results

Mesoproterozoic and Neoproterozoic (Pt_{2-3}) foliated quartz schist sample WC062715-4 has zircon populations of 1200–1000 Ma and 1600–1300 Ma, with two prominent peaks at ca. 1120 Ma and ca. 1445 Ma, respectively (Fig. 10A). A minor age population also occurs at Neoarchean ages (Fig. 10A). The three youngest zircons grains of this sample with overlapping ages have a weighted mean age of 1014 ± 18 Ma (MSWD = 0.53), which suggests an Upper Mesoproterozoic–Lower Neoproterozoic age for the Pt_{2-3} schist unit (Table 1).

Ordovician Qimen Tagh Group quartz schist sample WC071716-2 has zircon populations of

700–500 Ma and 1000–900 Ma, with two prominent peaks at ca. 620 Ma and ca. 940 Ma, respectively (Fig. 10B). Minor age populations also occur at 2000–1800Ma and 2650–2500 Ma, with peaks of 1920Ma and 2520 Ma, respectively (Fig. 10B). The three youngest zircons grains of this sample with overlapping ages have a weighted mean age of 507 ± 16 Ma (MSWD = 4.1), which suggests a Lower Ordovician age for the early Paleozoic rock unit (Table 1).

Lower Carboniferous Tuokuzidaban Group quartzite sample WC072715-4 has a main zircon population of 530-400 Ma, with prominent peak at ca. 440 Ma; minor age populations also occur at 1000-700 Ma, with a peak of ca. 900 Ma (Fig. 10C). The three youngest zircon grains from this sample with overlapping ages have a weighted mean age of $400 \pm 12 \text{ Ma}$ (MSWD = 7.0; Table 1). The Lower Carboniferous Tuokuzidaban Group slightly foliated sandstone sample WC072715-3 has a main zircon population of 500-355 Ma with prominent peak at ca. 408 Ma (Fig. 10D); the three youngest zircon grains from this sample with overlapping ages have a weighted mean age of 359 ± 8 Ma (MSWD = 7.0), which suggests a Lower Carboniferous age for the sedimentary rock unit (Table 1).

The Lower-Middle Jurassic Dameigou Formation coarse-grained sandstone sample WC062715-5 has a main zircon population of 510-400 Ma, with prominent peak at ca. 427 Ma, and a minor age peak also occurs at ca. 260 Ma (Fig. 10E). The three youngest zircon grains of this sample with overlapping ages have a weighted mean age of 242 ± 28 Ma (MSWD = 1.29; Table 1). Another medium- to fine-grained sandstone sample WC072715-1 has a zircon population of 320-220 Ma, with prominent peak at ca. 241 Ma, and a minor age peak also occurs at ca. 420 Ma (Fig. 10F). The three youngest zircon grains of this sample with overlapping ages have a weighted mean age of $227 \pm 7 \text{ Ma (MSWD} = 4.9; Table 1).$

The Upper Jurassic Caishiling Formation medium-grained sandstone sample WC072715-6 has a zircon population of 500-200 Ma, with two prominent peaks at ca. 225 Ma and ca. 405 Ma, and a minor age peak also occurs at ca. 1000 Ma (Fig. 10G). The three youngest zircon grains of this sample with overlapping ages have a weighted mean age of 193 ± 1 Ma (MSWD = 0.33; Table 1). Another pink-brown sandstone sample WC072715-7 has a zircon population of 480-200 Ma, with two prominent peaks at ca. 230 Ma and ca. 407 Ma, and a minor age peak also occurs at ca. 950 Ma (Fig. 10H). In addition, Paleoproterozoic-Neoarchean grains are present in this sample (Fig. 10H). The youngest single-zircon grain of this sample

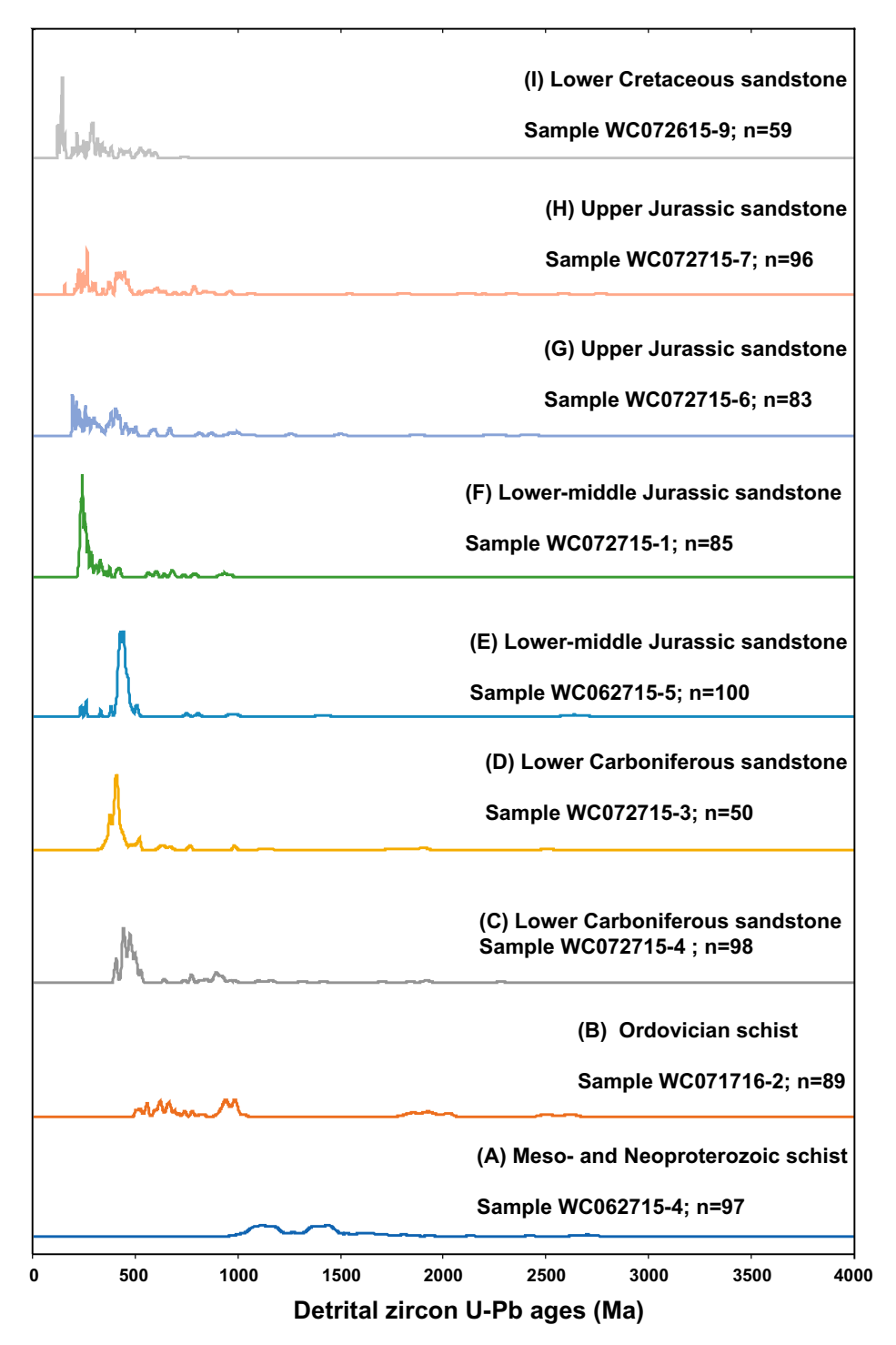


Figure 10. Normalized relative probability plots of detrital zircon U-Pb ages from the Mesoproterozoic and Neoproterozoic to Cretaceous sediments in the Qiemo River mapping area from this study. See Table DR2 (text footnote 1) for the detailed data set.

yielded a U-Pb age of 156 ± 2 Ma, which suggests an Upper Jurassic age for the sedimentary rock unit (Table 1).

Lower Cretaceous Quanshigou Formation sandstone sample WC072615-9 has zircon populations of 160–120 Ma and 300–200 Ma,

with two prominent peaks at ca. 144 Ma and ca. 240 Ma, respectively (Fig. 10I). A minor age population also occurs at 600–400 Ma, with a peak at 430 Ma (Fig. 10I). The three youngest zircon grains of this sample with overlapping ages have a weighted mean age of 124 ± 10 Ma

(MSWD = 0.66), which suggests a Lower Cretaceous age for the Mesozoic sedimentary rock unit (Table 1). In addition, a 3.5 Ga grain was present in this sample (Table DR2).

DISCUSSION

Stratigraphic and Provenance Analysis

Our new detrital zircon age data from this study can aid in detailed stratigraphic analysis for each geologic mapping unit and explore provenance implications that derive from comparisons between the previously published data sets and our paleocurrent data. The discussion is organized by age of deposition and is keyed to previous reconstructions for the preferred provenance interpretations.

The Kuhai Group, recognized as the old metamorphic basement of the western domain of the Eastern Kunlun Range, is locally exposed in the eastern portion of the mapping area. Our new geochronology result for a migmatite sample shows an upper-intercept weighted mean 207 Pb/ 206 Pb age of 1868 \pm 24 Ma (Fig. 8F), which we interpret as the age of protolith deposition. We suggest a Paleoproterozoic age for the basement of the western domain of the Eastern Kunlun Range (i.e., ca. 1.87 Ga). The Mesoproterozoic and Neoproterozoic schist yielded rather simple detrital zircon age spectra characterized by a large number of 1.2–1.0 Ga and 1.5– 1.3 Ga zircon grains (Fig. 10A). The younger component of this age range is correlative with plutonic rocks along the northern margins of the Kunlun-Qaidam terrane and Qilian Shan (e.g., Gehrels et al., 2003a, 2003b; Zhang et al., 2005; Wu et al., 2016a, 2017, 2018, 2019a; He et al., 2016a, 2016b, 2018; Liu et al., 2018, 2019; Zuza et al., 2018), whereas the older component of the age clustering at ca. 1.5-1.3 Ga is uniquely correlative to the Qilian Shan to the northeast, corresponding to the North China craton (Fig. 11; e.g., Wu et al., 2017; Liu et al., 2018, 2019; Zuza et al., 2018). Although 1.4 Ga A-type granites were reported in the south Tarim (Ye et al., 2016), the outcrop exposure was poor, and it was too far west from the study area. We suggest that the Mesoproterozoic and Neoproterozoic unit was deposited between ca. 1014 Ma and ca. 817 Ma based on our detrital zircon data (i.e., sample WC062715-4; Fig. 10A) and the intrusive relationships with the Neoproterozoic granitoid (i.e., sample WC072716-3; Fig. 8B).

The Lower Ordovician Qimen Tagh Group mainly formed age peaks at 700–500 Ma and 1.1–0.9 Ga (Fig. 10B). The younger component of this age range implies that the South Altyn Tagh Range and Qilian were not the main provenance areas, which is possibly correlative with

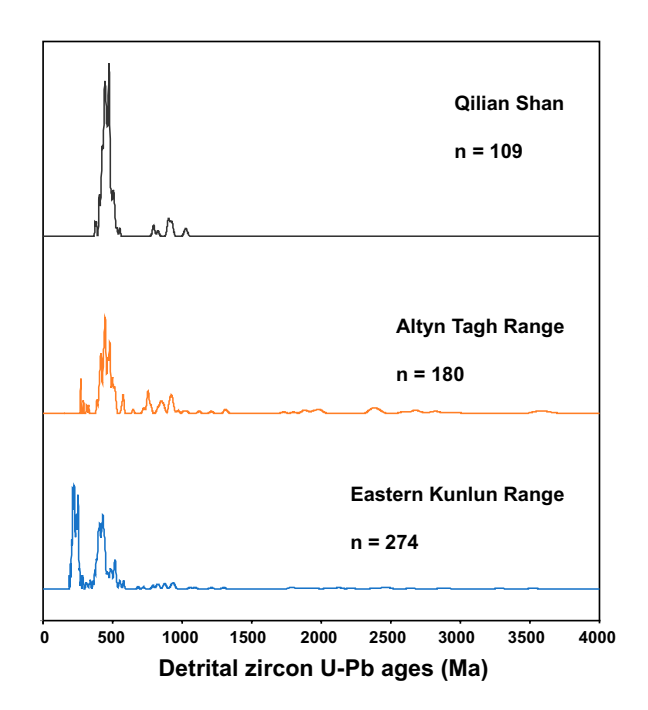


Figure 11. Normalized probability plot of zircon ages from the Eastern Kunlun Range, Qilian Shan, and Altyn Tagh Range. U-Pb ages were used for zircons younger than 1000 Ma, and Pb-Pb ages were used for older zircons, which correspond to widespread tectonic events as discussed in the text.

the Eastern Kunlun Range (e.g., Bian et al., 2000; Zhang et al., 2005), whereas the older component of the age clustering is uniquely correlative to the northern margins of the Kunlun-Qaidam terrane and Qilian Shan (e.g., Cowgill et al., 2003; Gehrels et al., 2003a; Zhang et al., 2005; Wu et al., 2016a, 2017, 2019a; He et al., 2016a, 2016b; Liu et al., 2018, 2019; Zuza et al., 2018). The minor Paleoproterozoic-late Archean zircon grains are the basement of north Tibet, which may possibly be derived from the Tarim-North China cratons (Wu et al., 2017, 2019a; Zuza et al., 2018; Liu et al., 2018, 2019). Both the Lower Carboniferous Tuokuzidaban Group samples yielded rather simple detrital zircon age spectra characterized by early Paleozoic zircon grains, which may possibly be derived from the South Altyn Tagh Range (e.g., Liu et al., 2015; Kang et al., 2016; C.L. Wu et al., 2016b; Zhu et al., 2019; this study) and western margin of the Eastern Kunlun Range (i.e., Qimen Tagh terrane; Fig. 11; e.g., C. Wu et al., 2016a; Yu et al., 2017; Dong et al., 2018). The Carboniferous zircon grains of these samples are uniquely correlative to the local plutonic rocks of the western domain of the Eastern Kunlun Range, i.e., Jianxia Shan pluton in the mapping area (i.e., sample WC071615-9; Fig. 5). We suggest that the Tuokuzidaban Group in the Eastern Kunlun Range was deposited at ca. 358 Ma, based on our detrital zircon data (i.e., samples WC072715-4 and WC072715-3; Figs. 10C and 10D) and the volcanic tuff sample (i.e., sample WC071516-2; Fig. 8A).

All four Jurassic sandstone samples show two prominent Phanerozoic age populations with

ca. 500-400 Ma and ca. 300-200 Ma groups (Figs. 10E-10H), corresponding to the bimodal age distribution characteristic of the Kunlun batholith (e.g., Cowgill et al., 2003; Gehrels et al., 2003a; C. Wu et al., 2016a). However, southward paleocurrent indicators in the Jurassic strata (Fig. 4) suggest that the South Tarim and/ or Altyn Tagh Range to the north acted as a possible source for the older component age cluster of these sediments (Fig. 11). However, the exact location of the Altyn Tagh Range in the Jurassic is unclear. Post-Jurassic left-lateral offset along the Altyn Tagh fault may imply that rocks exposed in the Altyn Tagh Range were located northeast of their present-day position, and thus may not have provided a source for Jurassic sediments. The Permian-Triassic zircon grains are uniquely correlative to the local plutonic rocks of the western margin of the Eastern Kunlun Range (e.g., Roger et al., 2003; Li et al., 2013; Wu et al., 2016a, 2019a). The Lower Cretaceous sandstone sample exhibits two significant populations at 160-120 Ma and 300-200 Ma (Fig. 10I), corresponding to the characteristic ages of the Eastern Kunlun Range. A third age population spans 600-400 Ma. Therefore, the Lower Cretaceous sediments were probably locally derived at the western domain of the Eastern Kunlun Range (Fig. 11; e.g., Zhang et al., 2005; Li et al., 2013; Wu et al., 2016a, 2019a).

Neoproterozoic-Mesozoic Tectonic Evolution of Northwestern Tibet

In the late Mesoproterozoic-early Neoproterozoic, sediments were deposited along the

southern and northern edges of the Altyn Tagh and Eastern Kunlun Ranges, respectively (Wu et al., 2016a, 2019a; Meng et al., 2017; Yu et al., 2017; this study). The sediments consisted of ca. 1.45 Ga and ca. 1.1 Ga detrital zircon grains derived from the linked Tarim-North China craton to the north and minor local granitoids (e.g., Gehrels et al., 2003b, 2003b; He et al., 2016a; Wu et al., 2016a, 2019a; this study). Early Neoproterozoic (i.e., ca. 0.9-1.0 Ga) magmatism across North Tibet was followed by local deformation (e.g., Wu et al., 2016a, 2017, 2019a; He et al., 2016b, 2018; Meng et al., 2017; Zuza and Yin, 2017; Zuza et al., 2018). Leucogranites and metamorphic zircon rims with ages of ca. 0.9-0.81 Ga in the Eastern Kunlun and South Altyn Tagh Ranges (i.e., ca. 817 Ma of sample WC072716-3; Fig. 8B; e.g., Gehrels et al., 2003a; Wu et al., 2017; Zuza et al., 2018; this study) are associated with the inferred collision between the linked North China-Tarim craton and the Songpan-Ganzi terrane by no later than ca. 750 Ma during closure of the proto-Kunlun ocean (e.g., Wu et al., 2016a, 2019a; Zuza and Yin, 2017). In the late Neoproterozoic, rifting of this joined continent initiated at variable times, resulting in the opening of the South Altyn Tagh and paleo-Kunlun oceans, from north to south, respectively (e.g., Wu et al., 2016a, 2019a; Zuza and Yin, 2017). The earliest phase of rifting and the opening of the paleo-Kunlun ocean initiated during or immediately following the aforementioned collision (e.g., Wu et al., 2016a, 2019a; Zuza and Yin, 2017; Zuza et al., 2018). The emplacement of ca. 733 Ma mafic dikes in the Eastern Kunlun Range associated with the development of a passive margin as diking was coeval with the deposition of the shallow-marine sequence (i.e., Wanbaogou Formation; Wu et al., 2016a, 2019a).

The onset of paleo-Kunlun ocean subduction along the southern margin of the Kunlun-Qaidam terrane could have occurred as early as the end of the Neoproterozoic (e.g., Jiang et al., 1992; Yang et al., 1996; Yin and Harrison, 2000; Mo et al., 2007; Wu et al., 2016a, 2019a), and protracted arc magmatism lasted until the Devonian (e.g., Yin and Harrison, 2000; Cowgill et al., 2003; Gehrels et al., 2003a; Chen et al., 2012; Wu et al., 2016a, 2019a). In the north, the oceanic crust of the Kunlun-Qaidam terrane began to subduct northward by ca. 520 Ma, creating a dominant Cambrian arc along the southern margin of the Altyn Tagh Range. This is evidenced by the emplacement of ca. 520-500 Ma I-type adakitic granitoid dikes in the South Altyn Tagh Range associated with the development of a passive margin coeval with the deposition of the shallow-marine sequence in the Eastern Kunlun Range (e.g., Wang et al., 2013; Wu et al.,

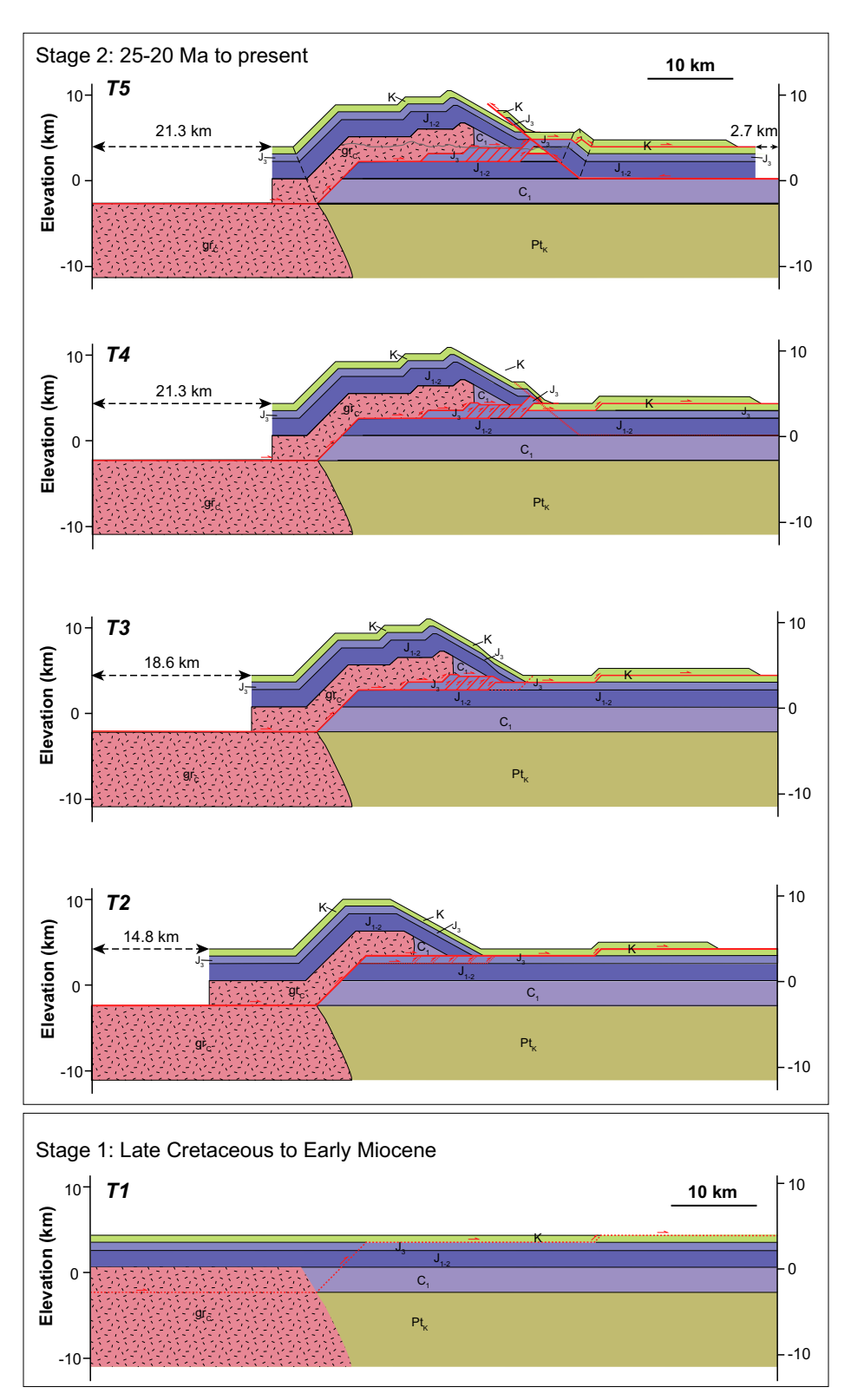


Figure 12. Structural balanced cross section of the Qiemo section (located in Fig. 5), showing section lengths, fault slip, and shortening magnitudes in two specific stages from T1 to T5. The strata symbols are the same as those in Figure 4; the gray line is the topographic line.

2016a, 2019a). A weak peraluminous granite with an age of ca. 495 Ma experienced peak metamorphism (Liu et al., 2015) as abundant metamorphic monazite was being formed (Zhu et al., 2019), suggesting that closure of the South Altyn Tagh ocean occurred at this time. The final closure of the subducted South Altyn Tagh ocean did not occur before the Middle Ordovician associated with the development of the ca. 480 and ca. 465 Ma Mangnai-Munabulake and Qingshuiquan ophiolites, from north to south, respectively (e.g., Liu et al., 2015; Zhu et al., 2019). Abundant ca. 460-445 Ma S-type granitoids provide further evidence for this interpretation (e.g., Cao et al., 2010; Yang et al., 2012; Kang et al., 2013; this study). The Late Silurian-Middle Devonian (i.e., ca. 426-385 Ma) alkaline granitoids suggest a postcollisional crustal extension setting in the South Altyn Tagh Range (e.g., Wu et al., 2007; C.L. Wu et al., 2014a; Liu et al., 2015; Wang et al., 2008a; Kang et al., 2016). If we restore Altyn Tagh offset, the rocks northwest of the Altyn Tagh fault in our study should get close to the Qilian Shan. We further demonstrate (1) that the geology on either side of the Altyn Tagh fault is different, (2) that the rocks to the north of the Altyn Tagh match or correlate with features in the Qilian Shan, such as the Qilian arc (e.g., Wu et al., 2017; Liu et al., 2018, 2019; Zuza et al., 2018), and (3) that the detrital zircon signatures differ between the existence and the closure of the South Altyn Tagh ocean.

Final consumption of the paleo-Kunlun ocean and continental collision occurred by 399-360 Ma, which is evidenced by the Late Devonian-early Carboniferous (ca. 360 Ma) metaluminous granite observed in the Eastern Kunlun Range (Wu et al., 2019a). Exhumation of the Late Devonian-early Carboniferous granitoids in the western domain of the Eastern Kunlun Range may have been associated with the syn- and postcollision processes between the Kunlun-Qaidam and Songpan-Ganzi terranes. However, the lack of a definitively recognizable geochemistry signature in this study makes this interpretation uncertain. Across the Eastern Kunlun Range, the wide belt of late Paleozoicearly Mesozoic arc plutons (i.e., granite sample WC071715-2 in this study) that generally young to the southwest can be explained by southward steepening of the subducting Paleo-Tethyan (also referred as the Neo-Kunlun) oceanic slab (Wu et al., 2016a, 2019a), which was induced by fluid-fluxing melting of an enriched lithospheric mantle (Chen et al., 2015; Wu et al., 2019a). The Mesozoic sediments in the western domain of the Eastern Kunlun Range were derived from the South Altyn Tagh Range to the north and local recycled material.

Cenozoic Deformation and Shortening Estimates across the Western Domain of the Eastern Kunlun Range

Our detailed mapping and structural analysis, presented in the form of a balanced cross section, provide quantitative estimates of the Cenozoic deformation that has affected northwestern Tibet. The ultimate goal of our field-based structural analyses and balanced cross-section restorations was to determine the kinematics of this region, which may have involved left-slip faulting related to the proximal Altyn Tagh fault and north-directed thrusting during widespread contractional deformation in central-northern Tibet (e.g., Meyer et al., 1998; Zuza et al., 2016, 2017; Allen et al., 2017). Balanced cross sections were constructed using Midland Valley's 2D Move software, and the restoration was developed using inverse kinematic modeling by this software package. Because of thick-skinned deformation and large variations/uncertainties in stratigraphic thicknesses, we used the linebalancing method to restore deformation, as opposed to an area balance (e.g., Chamberlin, 1923; Suppe, 1983; Mitra and Namson, 1989; Judge and Allmendinger, 2011).

Deformed-state cross sections were developed with a fault-bend fold geometry (Suppe, 1983). The construction of balanced cross sections relies on four assumptions: (1) The folding and rock uplifting are both controlled by the fault slip, (2) stratigraphic layers were originally horizontal before the deformation, (3) parallel folding is assumed to have been accommodated by flexural slip along bedding horizons, and (4) layer lengths and bed areas both remained constant during the deformation. In addition, we assumed dip-slip faulting on all thrust faults, which is reasonable based on our fault observations (Figs. 5 and 6). Complex overprinting dip-slip versus strike-slip deformation affected this region, and the most significant strike-slip shearing occurred in the Qiemo River valley, where exposed units consist of deformed Proterozoic rocks and ultramafic mélange. We did not attempt to quantitatively interpret the complex deformation in the Qiemo River valley because the lack of bedded units and abundant strike-slip shearing make any interpretations ambiguous and nonunique. The balanced cross section and kinematic restoration are only presented for the region just south of the Qiemo River, where deformation is predominately dip-slip, and Carboniferous-Cretaceous bedded strata provided geometric information to be included in the cross-section models. We acknowledge that the geology north of our section line A-A' was affected by out-of-plane left-lateral transpressional deformation associated with the Altyn Tagh fault (Fig. 5). Our cross section

of contractional strain outlined herein shows the minimum shortening required to produce the observed rock geometries and unit juxtapositions. That said, the significance of out-of-plane strikeslip deformation is unconstrained.

The balanced and restored cross-section models are presented in Figure 12. The deformedstate cross sections adhere to the map-view relationships and structural observations discussed above. The restoration of these sections involved restoring slip along the mapped faults to reposition the early-to-middle Mesozoic unconformity surfaces (e.g., the Early Jurassic unconformity horizon) back to horizontal. Pin lines were placed through undeformed strata. Additional cross-section-specific explanations are presented along with cross section in Figure 12. A detachment depth of at least ~14 km blow Earth's surface was calculated using areabalance methods for the western domain of the Eastern Kunlun Range cross section (Chu et al., 2009; Sloan et al., 2011; Zuza et al., 2018, 2019). This section shows a major thrust-wedge duplex (triangle-zone structure), and southeast-directed back-thrust in the northern part (Fig. 12). The Lower Carboniferous strata developed as a klippe in contact with the Upper Jurassic sediments in the middle, whereas the Cretaceous strata, which were first thrust over Jurassic rocks, are represented as a structural window beneath Jurassic rocks that were thrust over in a later phase (Figs. 5 and 12). The minimum magnitude of north-south shortening estimated from cross-section restoration is ~24 km (30% strain) for profiles A-A'.

The initiation age for this deformation is not constrained. The most direct evidence for shortening initiation is the truncation of Eocene terrestrial strata by thrust faults (Fig. 3). Based on sedimentological and thermochronology evidence, Wang et al. (2017) suggested a middle to later Eocene (i.e., ca. 40 Ma) deformation initiation age in the western domain of the Eastern Kunlun Range. Using this age yields a long-term shortening rate across the western domain of the Eastern Kunlun Range of 0.6 mm yr-1. Regionally, it is apparent that Cenozoic thrusting in northwest Tibet initiated locally at 50-45 Ma in the North Qaidam thrust belt, and deformation migrated southward to the Qimen Tagh thrust belt by 25-20 Ma (e.g., Jolivet et al., 2001, 2003; Yin et al., 2007, 2008a, 2008b; F. Cheng et al., 2017a; Shi et al., 2018; Wu et al., 2019b). Alternatively, if deformation initiated later at ca. 25-20 Ma, as in the western Eastern Kunlun thrust belt, the shortening rate would be 1.2-0.9 mm yr⁻¹. Given the range of initiation ages, the thrust belt experienced contractional strain rates of 4.7 $\times 10^{-16} \,\mathrm{s}^{-1}$ to $2.3 \times 10^{-16} \,\mathrm{s}^{-1}$, which overlap with established bulk Cenozoic strain rates across much of the Himalayan-Tibetan orogen (Clark, 2012; Zuza et al., 2019).

The ~24 km value of Cenozoic shortening (~30% strain) estimated via the restoration of the balanced cross section along our ~80 km traverse (Fig. 12) is comparable to regional shortening estimates across the region (Yin and Harrison, 2000; Yin et al., 2007, 2008a, 2008b). Yin et al. (2007) estimated a minimum of ~150 km of shortening (46% strain) across the Oimen Tagh-Yousha Shan thrust belt to the northeast. Compared to the west of the study area, X.G. Cheng et al. (2017b) estimated a minimum of ~27 km of shortening (~32% strain) across the Western Kunlun thrust belt. In a thesis, Yakovlev (2015) reported ~9 km (~20%) of shortening across a 36-km-long traverse of the Guaizi Liang range to the east of our study area. Integrated cosmogenic radionuclide dating suggests Quaternary shortening rates of ~1.7 mm/yr across the Yakovlev (2015) section, which is broadly comparable to our rates.

Because of their similar present-day physiography, we extrapolated these shortening magnitudes of ~20%-30%, from this and other studies (Yin et al., 2007; Yakovlev, 2015), over a ~100-km-long traverse across the Jianxia Shan to the Tula Basin, which yielded a minimum of Cenozoic 25-42 km of shortening. Whether this shortening initiated at ca. 40 Ma or 25-20 Ma yields north-south shortening rates of 0.6-1.1 mm/yr or 1.0-2.1 mm/yr, respectively. We note that these strain values could thicken crust that was originally ~40 km thick prior to the Cenozoic to thicknesses of 50-57 km, assuming pure-shear thickening and the rationale outlined in Zuza and Yin (2016). These values match present-day crustal thickness estimates based on receiver function data recorded by a large-scale dense array (i.e., Xu et al., 2013, 2018), which emphasizes that crustal shortening was sufficient here to thicken the crust.

North-south shortening can be converted to northeast-striking left-lateral shear through simple geometric arguments. The contribution of shortening magnitude, sh, to strike-slip shear, ss, is given by $ss = sh \sin(\theta)$, where θ is the angle between the strike of the thrust faults and the strike-slip faults. Given that our cross-section profile strikes north and the Altyn Tagh fault here strikes ~N70°E, strike-slip shear from ~25-42 km of shortening equates to $25-42 \text{ km} \times \sin (20^\circ) = 8.5-14.4 \text{ km}$. Similarly, shortening rates of 1 mm/yr to 2 mm/yr convert to 0.3-0.7 mm/yr. These calculations demonstrate that the contractional deformation observed in this study did not significantly contribute to left-slip offset on the Altyn Tagh fault, which has ~10 mm/yr slip rates (e.g., Cowgill et al., 2009).

CONCLUSIONS

The integrated results of our study involving detailed geologic mapping, structural analysis, balanced cross-section restoration, sedimentology, and new geochronology across the western domain of the Eastern Kunlun Range, together with existing work across northern Tibet, led to the following interpretations.

We suggest a Paleoproterozoic age for the basement of the western domain of the Eastern Kunlun Range, i.e., ca. 1.87 Ga, whereas the Mesoproterozoic and Neoproterozoic unit was deposited between ca. 1.0 Ga and ca. 0.82 Ga. The Lower Ordovician Qimen Tagh Group records a return to relatively local derivation from the Tuokuzidaban Group in the Eastern Kunlun Range, which was deposited at ca. 358 Ma based on our detrital zircon data and the volcanic tuff age. The detrital zircon results clearly distinguish the Early Ordovician Qimen Tagh Group schist from the Carboniferous sandstone samples, which were related to the evolution of the South Altyn Tagh Range. The southward paleocurrent indicators in the Jurassic strata imply that the South Tarim and/or Altyn Tagh Range to the north acted as a possible source for the older component age clusters of these sediments, and Cretaceous strata have contributions from local sources, with grains ultimately derived from the Kunlun orogenic systems.

Restoration of an ~56-km-long balanced cross section across the western domain of the Eastern Kunlun Range suggests that Cenozoic minimum shortening strain was ~30% (~24 km of shortening). Field evidence suggests that this shortened commenced after ca. 25–20 Ma, and the thrust belt experienced a shortening rate of 1.2–0.9 mm yr⁻¹ and strain rates of 4.7 × 10⁻¹⁶ s⁻¹ to 2.3 × 10^{-16} s⁻¹, which overlap with established Cenozoic strain rates across much of the Himalayan-Tibetan orogen. The contractional deformation observed in this study did not significantly contribute to left-slip offset on the Altyn Tagh fault, which has ~10 mm/yr slip rates.

ACKNOWLEDGMENTS

This research was made possible by grants from the National Science Foundation of China (41702232), and the Fundamental Research Funds for the Central Universities (C. Wu and C.F. Liu). This work was also supported by the China University of Geosciences (Beijing), a grant from the SINO-Probe Program administered by the Chinese Academy of Geological Sciences (SinoProbe-08-01), and the Qiemo Mapping Program administered by the Institute of Geological Survey (2016007907), China University of Geosciences (Beijing). The Tectonics Program of the U.S. National Science Foundation (EAR-1914501) is acknowledged for its support (A. Zuza). We appreciate Editor Brad Singer, the associate editor, and two anonymous reviewers for their critical, careful, and very constructive reviews that helped to improve the clarity and interpretations of the original draft. Yahui Yue, Di Xiu, Shuxiang Han, and Jialiang Li helped with analytical procedures. Midland Valley are acknowledged for the provision of the academic license of MOVE to University of Houston.

REFERENCES CITED

- Allen, M.B., Walters, R.J., Song, S., Saville, C., De Paola, N., and Ford, J., 2017, Partitioning of oblique convergence coupled to the fault locking behavior of fold-and-thrust belts: Evidence from the Qilian Shan, northeastern Tibetan Plateau: Tectonics, v. 36, p. 1679–1698, https:// doi.org/10.1002/2017TC004476.
- Arne, D., Worley, B., Wilson, C., Chen, S.F., Foster, D., Luo, Z.L., and Dirks, P., 1997, Differential exhumation in response to episodic thrusting along the eastern margin of the Tibetan Plateau: Tectonophysics, v. 280, no. 3-4, p. 239–256, https://doi.org/10.1016/S0040-1951(97)00040-1.
- Bendick, R., Bilham, R., Freymueller, J., Larson, K., and Yin, G., 2000, Geodetic evidence for a low slip rate in the Altyn Tagh fault system: Nature, v. 404, no. 6773, p. 69, https://doi.org/10.1038/35003555.
- Bian, Q., Luo, X.Q., Li, D.H., Zhao, D.S., Chen, H.H., Xu, G.Z., Chang, C.F., and Gao, Y.L., 2000, Discovery of Caledonian island-arc granodiorite-tonalite in Buqingshan, Qinghai Province: Progress in Natural Science, v. 10, p. 74–78.
- Bian, Q., Zhu, S., Semikhatov, I.I., Sun, S., Chen, D., and Na, C., 2005, Discovery of the Jiawengmen stromatolite assemblage in the southern belt of Eastern Kunlun, NW China, and its significance: Acta Geologica Sinica, v. 79, p. 471–480, https://doi.org/10.1111/j.1755-6724.2005.tb00913.x.
- Burchfiel, B.C., Deng, Q., Molnar, P., Royden, L., Wang, Y., Zhang, P., and Zhang, W., 1989, Intracrustal detachment within zones of continental deformation: Geology, v. 17, p. 748–752, https://doi.org/10.1130/0091-7613(1989)017<0448:IDWZOC>2.3.CO;2.
- Burchfiel, B.C., Zhang, P., Wang, Y., Zhang, W., Song, F., Deng, Q., Molnar, P., and Royden, L., 1991, Geology of the Haiyuan fault zone, Ningxia-Hui Autonomous Region, China, and its relation to the evolution of the northeastern margin of the Tibetan Platea: Tectonics, v. 10, no. 6, p. 1091–1110, https://doi.org/10.1029/90TC02685.
- Cao, Y.T., Liu, L., Wang, C., Yang, W.Q., and Zhu, X.H., 2010, Geochemical zircon U-Pb dating and Hf isotope compositions studies for Tatelekebulake granite in South Altyn Tagh: Acta Petrologica Sinica (Yanshi Xuebao), v. 26, p. 3259–3271 [in Chinese with English abstract].
- Cao, Y.T., Liu, L., Wang, C., Kang, L., Yang, W.Q., Liang, S., Liao, X.Y., and Wang, Y.W., 2013, Determination and implication of the HP pelitic granulite from the Munabulake area in the South Altyn Tagh: Acta Petrologica Sinica (Yanshi Xuebao), v. 29, no. 5, p. 1727–1739 [in Chinese with English abstract].
- Chamberlin, R.T., 1923, On the crustal shortening of the Colorado Rockies: American Journal of Science, v. 5–6, no. 33, p. 215–221, https://doi.org/10.2475/ajs. s5-6.33.215.
- Che, Z., Liu, L., and Luo, J.H., 1995, The discovery and occurrence of high-pressure metamorphic rocks from Altyn Mountain area, Xinjiang Autonomous Region: Chinese Science Bulletin, v. 40, p. 1298–1300 [in Chinese].
- Che, Z.C., and Sun, Y., 1996, The age of the Altun granulite facies complex and the basement of the Tarim basin: Reginal Geology of China, v. 56, p. 51–57 [in Chinese with English abstract].
- Chen, W.P., Chen, C.Y., and Nabelek, J.L., 1999, Present-day deformation of the Qaidam Basin with implications for intra-continental tectonics: Tectonophysics, v. 305, p. 165–181, https://doi.org/10.1016/S0040-1951(99)00006-2.
- Chen, X.H., Yin, A., Gehrels, G.E., Cowgill, E.S., Grove, M., Harrison, T.M., and Wang, X.F., 2003, Two phases of Mesozoic north-south extension in the eastern Altyn Tagh range, northern Tibetan Plateau: Tectonics, v. 22, 1053, https://doi.org/10.1029/2001TC001336.

- Chen, X.H., Gehrels, G.E., Yin, A., Li, L., and Jiang, R.B., 2012, Paleozoic and Mesozoic basement magmatisms of eastern Qaidam Basin, northern Qinghai–Tibet Plateau: LA-ICP-MS zircon U-Pb geochronology and its geological significance: Acta Geologica Sinica, v. 86, p. 350–369, https://doi.org/10.1111/j.1755-6724.2012.00665.x.
- Chen, X.H., Gehrels, G.E., Yin, A., Zhou, Q., and Huang, P.H., 2015, Geochemical and Nd-Sr-Pb-O isotopic constraints on Permo-Triassic magmatism in eastern Qaidam Basin, northern Qinghai-Tibetan Plateau: Implications for the evolution of the Paleo-Tethys: Journal of Asian Earth Sciences, v. 114, p. 674–692, https://doi .org/10.1016/j.jseaes.2014.11.013.
- Cheng, F., Jolivet, M., Hallot, E., Zhang, D., Zhang, C., and Guo, Z., 2017a, Tectono-magmatic rejuvenation of the Qaidam craton, northern Tibet: Gondwana Research, v. 49, p. 248–263, https://doi.org/10.1016/ j.gr.2017.06.004.
- Cheng, X.G., Chen, H., Lin, X., Wu, L., and Gong, J., 2017b, Geometry and kinematic evolution of the Hotan-Tiklik segment of the western Kunlun thrust belt: Constrained by structural analyses and apatite fission track thermochronology: The Journal of Geology, v. 125, no. 1, p. 65–82, https://doi.org/10.1086/689187.
- Chu, R., Zhu, L., and Helmberger, D.V., 2009, Determination of earthquake focal depths and source time functions in central Asia using teleseismic P waveforms: Geophysical Research Letters, v. 36, no. 17, L17317, https://doi .org/10.1029/2009GL039494.
- Clark, M.K., 2012, Continental collision slowing due to viscous mantle lithosphere rather than topography: Nature, v. 483, p. 74–77, https://doi.org/10.1038/nature10848.
- Clark, M.K., and Royden, L.H., 2000, Topographic ooze: Building the eastern margin of Tibet by lower crustal flow: Geology, v. 28, no. 8, p. 703–706, https://doi .org/10.1130/0091-7613(2000)28<703:TOBTEM>2. 0.CO:2.
- Clark, M.K., Farley, K.A., Zheng, D., Wang, Z., and Duvall, A.R., 2010, Early Cenozoic faulting of the northern Tibetan Plateau margin from apatite (U-Th)/He ages: Earth and Planetary Science Letters, v. 296, no. 1-2, p. 78–88, https://doi.org/10.1016/j.epsl.2010.04.051.
- Cowgill, E., 2007, Impact of riser reconstructions on estimation of secular variation in rates of strike-slip faulting: Revisiting the Cherchen River site along the Altyn Tagh fault, NW China: Earth and Planetary Science Letters, v. 254, no. 3-4, p. 239–255, https://doi.org/10.1016/j.epsl.2006.09.015.
- Cowgill, E., Yin, A., Wang, X.F., and Zhang, Q., 2000, Is the North Altyn fault part of a strike-slip duplex along the Altyn Tagh fault system?: Geology, v. 28, p. 255–258, https://doi.org/10.1130/0091-7613(2000)28<255:ITNA FP>2.0.CO:2.
- Cowgill, E., Yin, A., Harrison, T.M., and Wang, X.F., 2003, Reconstruction of the Altyn Tagh fault based on U-Pb geochronology: Role of back thrusts, mantle sutures, and heterogeneous crustal strength in forming the Tibetan Plateau: Journal of Geophysical Research, v. 108, 2346, https://doi.org/10.1029/2002JB002080.
- Cowgill, E., Yin, A., Arrowsmith, J.R., Feng, W.X., and Shuanhong, Z., 2004, The Akato Tagh bend along the Altyn Tagh fault, northwest Tibet 1: Smoothing by vertical-axis rotation and the effect of topographic stresses on bend-flanking faults: Geological Society of America Bulletin, v. 116, no. 11-12, p. 1423–1442, https://doi .org/10.1130/B25359.1.
- Cowgill, E., Gold, R.D., Xuanhua, C., Xiao-Feng, W., Arrowsmith, J.R., and Southon, J., 2009, Low Quaternary slip rate reconciles geodetic and geologic rates along the Altyn Tagh fault, northwestern Tibet: Geology, v. 37, no. 7, p. 647–650, https://doi.org/10.1130/G25623A.1.
- DeCelles, P.G., Robinson, D.M., and Zandt, G., 2002, Implications of shortening in the Himalayan fold-thrust belt for uplift of the Tibetan Plateau: Tectonics, v. 21, no. 6, p. 12-1–12-25, https://doi.org/10.1029/2001TC001322.
- Dewey, J.F., and Burke, K.C., 1973, Tibetan, Variscan, and Precambrian basement reactivation: Products of continental collision: The Journal of Geology, v. 81, no. 6, p. 683–692, https://doi.org/10.1086/627920.
- Dewey, J.F., Shackleton, R.M., Chengfa, C., and Yiyin, S., 1988, The tectonic evolution of the Tibetan Plateau: Philosophical Transactions of the Royal Society of

- London, ser. A, Mathematical and Physical Sciences, v. 327, no. 1594, p. 379–413, https://doi.org/10.1098/rsta.1988.0135.
- Dickinson, W.R., 1970, Interpreting detrital modes of greywacke and arkose: Journal of Sedimentary Research, v. 40, p. 695–707.
- Dickinson, W.R., 1985, Interpreting provenance relations from detrital modes of sandstones, in Zuffa, G.G., ed., Provenance of Arenites: North Atlantic Treaty Organization (NATO) Advanced Study Institute (ASI) Series C Volume 148: Dordrecht, Netherlands, D. Reidel Publishing Company, p. 333–361, https://doi .org/10.1007/978-94-017-2809-6_15.
- Dickinson, W.R., and Suczek, C.A., 1979, Plate tectonics and sandstone compositions: American Association of Petroleum Geologists Bulletin, v. 63, no. 12, p. 2164– 2182.
- Dickinson, W.R., Beard, L.S., Brakenridge, G.R., Erjavec, J.L., Ferguson, R.C., Inman, K.F., and Ryberg, P.T., 1983, Provenance of North American Phanerozoic sandstones in relation to tectonic setting: Geological Society of America Bulletin, v. 94, no. 2, p. 222–235, https://doi.org/10.1130/0016-7606(1983)94<222:PON APS>2.0.CO:2.
- Ding, L., and Lai, Q., 2003, New geological evidence of crustal thickening in the Gangdese block prior to the Indo-Asian collision: Chinese Science Bulletin, v. 48, no. 15, p. 1604–1610, https://doi.org/10.1007/ BF03183969.
- Dong, Y., He, D., Sun, S., Liu, X., Zhou, X., Zhang, F., and Li, J., 2018, Subduction and accretionary tectonics of the East Kunlun orogen, western segment of the Central China orogenic system: Earth-Science Reviews, v. 186, p. 231–261, https://doi.org/10.1016/ j.earscirev.2017.12.006.
- Dong, Z.C., Xiao, P.X., Xi, R.G., Guo, L., and Gao, X.F., 2011, Geochemical characteristics and isotopic dating of bojites in the tectonic mélange belt on the south margin of Altun: Geological Review (Dizhi Lunping), v. 57, no. 2, p. 207–216.
- Dupont-Nivet, G., Robinson, D., Butler, R.F., Yin, A., and Melosh, H.J., 2004, Concentration of crustal displacement along a weak Altyn Tagh fault: Evidence from paleomagnetism of the northern Tibetan Plateau: Tectonics, v. 23, no. 1, TC1020, https://doi.org/10.1029/2002TC001397.
- Duvall, A.R., Clark, M.K., van der Pluijm, B.A., and Li, C., 2011, Direct dating of Eocene reverse faulting in northeastern Tibet using Ar-dating of fault clays and lowtemperature thermochronometry: Earth and Planetary Science Letters, v. 304, no. 3-4, p. 520–526, https://doi .org/10.1016/j.epsl.2011.02.028.
- Duvall, A.R., Clark, M.K., Kirby, E., Farley, K.A., Craddock, W.H., Li, C., and Yuan, D.Y., 2013, Low-temperature thermochronometry along the Kunlun and Haiyuan faults, NE Tibetan Plateau: Evidence for kinematic change during late-stage orogenesis: Tectonics, v. 32, no. 5, p. 1190–1211, https://doi.org/10.1002/tect.20072.
- Egan, S.S., Buddin, T.S., Kane, S.J., and Williams, G.D., 1997, Three-dimensional modelling and visualisation instructural geology: New techniques for the restoration and balancing of volumes, in Proceedings of the 1996 Geoscience Information Group Conference on Geological Visualisation: Electronic Geology, v. 1, no. 7, p. 67–82.
- England, P., and Houseman, G., 1986, Finite strain calculations of continental deformation: 2. Comparison with the India-Asia collision zone: Journal of Geophysical Research–Solid Earth, v. 91, no. B3, p. 3664–3676, https://doi.org/10.1029/JB091iB03p03664.
- England, P., and Houseman, G., 1989, Extension during continental convergence, with application to the Tibetan Plateau: Journal of Geophysical Research–Solid Earth, v. 94, no. B12, p. 17,561–17,579, https://doi. org/10.1029/JB094iB12p17561.
- England, P., and Searle, M., 1986, The Cretaceous–Tertiary deformation of the Lhasa block and its implications for crustal thickening in Tibet: Tectonics, v. 5, no. 1, p. 1–14, https://doi.org/10.1029/TC005i001p00001.
- Fraser, J.E., Searle, M.P., Parrish, R.R., and Noble, S.R., 2001, Chronology of deformation, metamorphism, and magmatism in the southern Karakoram Mountains: Geological Society of America Bulletin, v. 113,

- no. 11, p. 1443–1455, https://doi.org/10.1130/0016-7606(2001)113<1443:CODMAM>2.0.CO;2.
- Fu, B., Awata, Y., Du, J., and He, W., 2005, Late Quaternary systematic stream offsets caused by repeated large seismic events along the Kunlun fault, northern Tibet: Geomorphology, v. 71, no. 3-4, p. 278–292, https://doi .org/10.1016/j.geomorph.2005.03.001.
- Fu, B.H., and Awata, Y., 2007, Displacement and timing of left-lateral faulting in the Kunlun fault zone, northern Tibet, inferred from geologic and geomorphic features: Journal of Asian Earth Sciences, v. 29, no. 2-3, p. 253– 265, https://doi.org/10.1016/j.jseaes.2006.03.004.
- Gaudemer, Y., Tapponnier, P., Meyer, B., Peltzer, G., Shunmin, G., Zhitai, C., Huagung, D., and Cifuentes, I., 1995, Partitioning of crustal slip between linked, active faults in the eastern Qilian Shan, and evidence for a major seismic gap, the 'Tianzhu gap,' on the western Haiyuan fault, Gansu (China): Geophysical Journal International, v. 120, p. 599–645, https://doi.org/10.1111/j.1365-246X.1995.tb01842.x.
- Gehrels, G.E., Yin, A., and Wang, X.F., 2003a, Magmatic history of the Altyn Tagh, Nan Shan, and Qilian Shan region of western China: Journal of Geophysical Research, v. 108, p. 2423, https://doi.org/10.1029/2002JB001876.
- Gehrels, G.E., Yin, A., and Wang, X.F., 2003b, Detrital-zircon geochronology of the northeastern Tibetan Plateau: Geological Society of America Bulletin, v. 115, no. 7, p. 881–896, https://doi.org/10.1130/0016-7606(2003)115<0881:DGOTNT>2.0.CO;2.
- Gehrels, G.E., Kapp, P., DeCelles, P., Pullen, A., Blakey, R., Weislogel, A., Ding, L., Guynn, J., Martin, A., McQuarrie, N., and Yin, A., 2011, Detrital zircon geochronology of pre-Tertiary strata in the Tibetan-Himalayan orogen: Tectonics, v. 30, TC5016, https:// doi.org/10.1029/2011TC002868.
- Guo, Z.J., Zhang, Z.C., and Wang, J.J., 1999, Sm-Nd isochron age of ophiolite along northern margin of Altun Tagh Mountain and its tectonic significance: Chinese Science Bulletin, v. 44, p. 456–458, https:// doi.org/10.1007/BF02977887.
- Hao, J., Wang, E.Q., Liu, X.H., and Sang, H.Q., 2006, Jinyanshan collisional orogenic belt of the early Paleozoic in the Altun mountains: Evidence from single zircon U-Pb and 40Ar/39Ar isotopic dating for the arc magmatite and ophiolitic mélange: Acta Petrologica Sinica (Yanshi Xuebao), v. 22, no. 11, p. 2743–2752.
- Haproff, P.J., Zuza, A.V., Yin, A., Harrison, T.M., Manning, C.E., Dubey, C.S., Ding, L., Wu, C., and Chen, J.L., 2019, Geologic framework of the northern Indo-Burma Ranges and lateral correlation of Himalayan-Tibetan lithologic units across the eastern Himalayan syntaxis: Geosphere, v. 15, no. 3, p. 856–881.
- Harris, N.B.W., Xu, R., Lewis, C.L., Hawkesworth, C.J., and Zhang, Y., 1988, Isotope geochemistry of the 1985 Tibet Geotraverse, Lhasa to Golmud: Philosophical Transactions of the Royal Society of London, ser. A, Mathematical and Physical Sciences, v. 327, p. 263– 285, https://doi.org/10.1098/rsta.1988.0129.
- Harrison, T.M., Copeland, P., Kidd, W.S.F., and Yin, A.N., 1992, Raising Tibet: Science, v. 255, no. 5052, p. 1663– 1670, https://doi.org/10.1126/science.255.5052.1663.
- He, D., Dong, Y., Liu, X., Yang, Z., Sun, S., Cheng, B., and Li, W., 2016a, Tectono-thermal events in east Kunlun, northern Tibetan Plateau: Evidence from zircon U-Pb geochronology: Gondwana Research, v. 30, p. 179– 190, https://doi.org/10.1016/j.gr.2015.08.002.
- He, D., Dong, Y., Zhang, F., Yang, Z., Sun, S., Cheng, B., Zhou, B., and Liu, X., 2016b, The 1.0 Ga S-type granite in the East Kunlun orogen, northern Tibetan Plateau: Implications for the Meso- to Neoproterozoic tectonic evolution: Journal of Asian Earth Sciences, v. 130, p. 46–59, https://doi.org/10.1016/j.jseaes.2016.07.019.
- He, D., Dong, Y., Liu, X., Zhou, X., Zhang, F., and Sun, S., 2018, Zircon U-Pb geochronology and Hf isotope of granitoids in East Kunlun: Implications for the Neoproterozoic magmatism of the Qaidam block, northern Tibetan Plateau: Precambrian Research, v. 314, p. 377– 393, https://doi.org/10.1016/j.precamres.2018.06.017.
- Ingersoll, R. V., Bullard, T.F., Ford, R.L., Grimm, J.P., Pickle, J.D., and Sares, S.W., 1984, The effect of grain size on detrital modes: A test of the Gazzi-Dickinson pointcounting method: Journal of Sedimentary Petrology, v. 54, p. 103–116.

- Jackson, S.E., Pearson, N.J., Griffin, W.L., and Belousova, E.A., 2004, The application of laser ablation-inductively coupled plasma-mass spectrometry to in situ U-Pb zircon geochronology: Chemical Geology, v. 211, p. 47–69, https://doi.org/10.1016/j.chemgeo.2004.06.017.
- Jiang, C.F., Yang, J.S., Feng, B.G., Zhu, Z.Z., Zhao, M., Chai, Y.C., Shi, X.D., Wang, H.D., and Ha, J.Q., 1992, Opening and Closing Tectonics of Kunlun Mountains: Geological Memoirs: Beijing, Geological Publishing House, 224 p. [in Chinese with English abstract].
- Jolivet, M., Brunel, M., Seward, D., Xu, Z., Yang, J., Roger, F., and Wu, C., 2001, Mesozoic and Cenozoic tectonics of the northern edge of the Tibetan Plateau: Fission-track constraints: Tectonophysics, v. 343, no. 1-2, p. 111–134, https://doi.org/10.1016/S0040-1951(01)00196-2.
- Jolivet, M., Brunel, M., Seward, D., Xu, Z., Yang, J., Malavieille, J., Roger, F., Leyreloup, A., Arnaud, N., and Wu, C., 2003, Neogene extension and volcanism in the Kunlun fault zone, northern Tibet: New constraints on the age of the Kunlun fault: Tectonics, v. 22, 1052, https://doi.org/10.1029/2002TC001428.
- Judge, P.A., and Allmendinger, R.W., 2011, Assessing uncertainties in balanced cross sections: Journal of Structural Geology, v. 33, no. 4, p. 458–467, https://doi.org/10.1016/j.jsg.2011.01.006.
- Kang, L., Liu, L., Cao, Y.T., Wang, C., Yang, W.Q., and Zhu, X.H., 2011, Geochemistry, zircon LA-ICP-MS U-Pb ages and Hf isotopes of Hongliugou moyite from north Altyn Tagh tectonic belt: Geological Bulletin of China, v. 30, p. 1066–1076 [in Chinese with English abstract].
- Kang, L., Liu, L., Cao, Y.T., Wang, C., Yang, W.Q., and Liang, S., 2013, Geochemistry, zircon U-Pb age and its geological significance of the gneissic granite from the eastern segment of the Tatelekebulake composite granite in the south Altyn Tagh: Acta Petrologica Sinica (Yanshi Xuebao), v. 29, p. 3039–3048 [in Chinese with English abstract].
- Kang, L., Xiao, P.X., Gao, X.F., Xi, R.G., and Yang, Z.C., 2016, Early Paleozoic magmatism and collision orogenic process of the South Altyn: Acta Geologica Sinica, v. 90, p. 2527–2550 [in Chinese with English abstract].
- Kapp, P., Yin, A., Harrison, T.M., and Ding, L., 2005, Cretaceous—Tertiary shortening, basin development, and volcanism in central Tibet: Geological Society of America Bulletin, v. 117, no. 7-8, p. 865–878, https://doi.org/10.1130/B25595.1.
- Kapp, P., DeCelles, P.G., Gehrels, G.E., Heizler, M., and Ding, L., 2007, Geological records of the Lhasa-Qiangtang and Indo-Asian collisions in the Nima area of central Tibet: Geological Society of America Bulletin, v. 119, no. 7-8, p. 917–933, https://doi.org/10.1130/B26033.1.
- Kidd, W.S., and Molnar, P., 1988, Quaternary and active faulting observed on the 1985 Academia Sinica–Royal Society Geotraverse of Tibet: Philosophical Transactions of the Royal Society of London, ser. A, Mathematical and Physical Sciences, v. 327, no. 1594, p. 337–363, https://doi.org/10.1098/rsta.1988.0133.
- Kong, X., Yin, A., and Harrison, T.M., 1997, Evaluating the role of preexisting weaknesses and topographic distributions in the Indo-Asian collision by use of a thin-shell numerical model: Geology, v. 25, no. 6, p. 527–530, https://doi.org/10.1130/0091-7613(1997)025<0527:ET ROPW>2.3.CO;2.
- Lease, R.O., Burbank, D.W., Zhang, H., Liu, J., and Yuan, D., 2012, Cenozoic shortening budget for the northeastern edge of the Tibetan Plateau: Is lower crustal flow necessary?: Tectonics, v. 31, no. 3, TC3011, https://doi .org/10.1029/2011TC003066.
- Li, L., Li, A., Murphy, M.A., and Fu, Y.V., 2016, Radial anisotropy beneath northeast Tibet: Implications for lithosphere deformation at a restraining bend in the Kunlun fault and its vicinity: Geochemistry Geophysics Geosystems, v. 17, no. 9, p. 3674–3690, https://doi .org/10.1002/2016GC006366.
- Li, L., Wu, C., and Yu, X., 2018, Cenozoic evolution of the Altyn Tagh and East Kunlun fault zones inferred from detrital garnet, tourmaline and rutile in southwestern Qaidam Basin (northern Tibetan Plateau): Basin Research, v. 30, no. 1, p. 35–58, https://doi.org/10.1111/ bre.12241.

- Li, R.B., Pei, X.Z., Li, Z.C., Pei, L., Chen, Y.X., Liu, C.J., and Liu, T.J., 2015, The depositional sequence and prototype basin for Lower Triassic Hongshuichuan Formation in the eastern segment of East Kunlun Mountains: Geological Bulletin of China, v. 34, no. 12, p. 2302– 2314 [in Chinese with English abstract].
- Li, W., Neubauer, F., Liu, Y.J., Genser, J., Ren, S.M., Han, G.Q., and Liang, C.Y., 2013, Paleozoic evolution of the Qimantagh magmatic arcs, Eastern Kunlun Mountains: Constraints from zircon dating of granitoids and modern river sands: Journal of Asian Earth Sciences, v. 77, p. 183–202, https://doi.org/10.1016/ j.jseaes.2013.08.030.
- Liu, C.F., Wu, C., Zhou, Z., Yan, Z., Jiang, T., Song, Z., and Zhang, H., 2018, U-Pb detrital zircon geochronology from the basement of the Central Qilian terrane: Implications for tectonic evolution of northeastern Tibetan Plateau: International Journal of Earth Sciences, v. 107, no. 2, p. 673–686, https://doi.org/10.1007/s00531-017-1522-5.
- Liu, C.F., Wu, C., Song, Z., Liu, W., and Zhang, H., 2019, Petrogenesis and tectonic significance of early Paleozoic magmatism in the northern margin of the Qilian block, northeastern Tibetan Plateau: Lithosphere, v. 11, no. 3, p. 365–385, https://doi.org/10.1130/L1047.1.
- Liu, L., Che, Z.C., Wang, Y., Luo, J.H., Wang, J.Q., and Gao, Z.J., 1998, The evidence of Sm-Nd isochron age for the early Paleozoic ophiolite in Mangya area, Altun Mountains: Chinese Science Bulletin, v. 43, p. 754–756 [in Chinese with English abstract], https://doi.org/10.1007/ BF02898953.
- Liu, L., Che, Z.C., Wang, Y., Luo, J., and Chen, D.L., 1999, The petrological characters and geotectonic setting of high-pressure metamorphic rocks belt in Altyn Mountain: Acta Petrologica Sinica (Yanshi Xuebao), v. 15, p. 57–64 [in Chinese with English abstract].
- Liu, L., Zhang, A.D., Chen, D.L., Yang, J.X., Luo, J.H., and Wang, C., 2007, Implications based on LA-ICP-MS zircon U-Pb ages of eclogite and its country rock from Jianggalesayi area, Altyn Tagh: Earth Science Frontiers, v. 14, p. 98–107, https://doi.org/10.1016/S1872-5791(07)60004-9.
- Liu, L., Wang, C., Chen, D., Zhang, A., and Liou, J.G., 2009, Petrology and geochronology of HP-UHP rocks from the South Altyn Tagh, northwestern China: Journal of Asian Earth Sciences, v. 35, no. 3-4, p. 232–244, https://doi.org/10.1016/j.jseaes.2008.10.007.
- Liu, L., Wang, C., Cao, Y.T., Chen, D.L., Kang, L., Yang, W.Q., and Zhu, X.H., 2012, Geochronology of multistage metamorphic events: Constraints on episodic zircon growth from the UHP eclogite in the South Altyn, NW China: Lithos, v. 136, p. 10–26, https://doi.org/10.1016/j.lithos.2011.09.014.
- Liu, L., Kang, L., Cao, Y., and Yang, W., 2015, Early Paleozoic granitic magmatism related to the processes from subduction to collision in South Altyn, NW China: Science China–Earth Sciences, v. 58, no. 9, p. 1513–1522, https://doi.org/10.1007/s11430-015-5151-1.
- Liu-Zeng, J., Tapponnier, P., Gaudemer, Y., and Ding, L., 2008, Quantifying landscape differences across the Tibetan Plateau: Implications for topographic relief evolution: Journal of Geophysical Research— Earth Surface, v. 113, no. F4, F04018, https://doi.org/10.1029/2007JF000897.
- Lu, H., and Xiong, S., 2009, Magnetostratigraphy of the Dahonggou section, northern Qaidam Basin, and its bearing on Cenozoic tectonic evolution of the Qilian Shan and Altyn Tagh fault: Earth and Planetary Science Letters, v. 288, no. 3-4, p. 539–550, https://doi .org/10.1016/j.epsl.2009.10.016.
- Lu, L., Zhang, K.J., Yan, L.L., Jin, X., and Zhang, Y.X., 2017, Was Late Triassic Tanggula granitoid (central Tibet, western China): A product of melting of underthrust Songpan-Ganzi flysch sediments?: Tectonics, v. 36, p. 902–928, https://doi.org/10.1002/2016TC004384.
- Ludwig, K.R., 2003, Isoplot 3.00: Berkeley Geochronology Center Special Publication 4, 70 p.
- Meng, F.C., Jia, L.H., Ren, Y.F., Liu, Q., and Duan, X.P., 2017, Magmatic and metamorphic events recorded in the gneisses of the Wenquan region, East Kunlun Mountains, Northwest China: Evidence from the zircon U-Pb geochronology: Acta Petrologica Sinica (Yanshi Xuebao), v. 33, no. 12, p. 3691–3709 [in Chinese with English abstract].

- Mériaux, A.S., Ryerson, F.J., Tapponnier, P., Van der Woerd, J., Finkel, R.C., Xu, X., and Caffee, M.W., 2004, Rapid slip along the central Altyn Tagh fault: Morphochronologic evidence from Cherchen He and Sulamu Tagh: Journal of Geophysical Research—Solid Earth, v. 109, no. B6, B06401, https://doi.org/10.1029/2003JB002558.
- Mériaux, A.S., Tapponnier, P., Ryerson, F.J., Xiwei, X., King, G., Van der Woerd, J., and Wenbin, C., 2005, The Aksay segment of the northern Altyn Tagh fault: Tectonic geomorphology, landscape evolution, and Holocene slip rate: Journal of Geophysical Research— Solid Earth, v. 110, no. B4, B04404, https://doi.org/10.1029/2004JB003210.
- Meyer, B., Tapponnier, P., Gaudemer, Y., Peltzer, G., Shunmin, G., and Zhitai, C., 1996, Rate of left-lateral movement along the easternmost segment of the Altyn Tagh fault, east of 96°E (China): Geophysical Journal International, v. 124, no. 1, p. 29–44, https://doi.org/10.1111/j.1365-246X.1996.tb06350.x.
- Meyer, B., Tapponnier, P., Bourjot, L., Metivier, F., Gaudemer, Y., Peltzer, G., Shunmin, G., and Zhitai, C., 1998, Crustal thickening in Gansu-Qinghai, lithospheric mantle subduction, and oblique, strike-slip controlled growth of the Tibet Plateau: Geophysical Journal International, v. 135, p. 1–47, https://doi.org/10.1046/j.1365-246X.1998.00567.x.
- Mitra, S., and Namson, J.S., 1989, Equal-area balancing: American Journal of Science, v. 289, no. 5, p. 563–599, https://doi.org/10.2475/ajs.289.5.563.
- Mo, X.X., Luo, Z.H., Deng, J.F., Yu, X.H., Liu, C.D., Chen, H.W., Yuan, W.M., and Liu, Y.H., 2007, Granitoids and crustal growth in the east Kunlun orogenic belt: Geological Journal of China Universities, v. 3, p. 403–414 [in Chinese with English abstract].
- Mock, C., Arnaud, N.O., and Cantagrel, J.M., 1999, An early unroofing in northeastern Tibet? Constraints from 40Ar/39Ar thermochronology on granitoids from the Eastern Kunlun Range (Qianghai, NW China): Earth and Planetary Science Letters, v. 171, p. 107–122, https://doi.org/10.1016/S0012-821X(99)00133-8.
- Molnar, P., and Tapponnier, P., 1975, Cenozoic tectonics of Asia: Effects of a continental collision: Science, v. 189, no. 4201, p. 419–426, https://doi.org/10.1126/ science.189.4201.419.
- Murphy, M.A., Yin, A., Harrison, T.M., Dürr, S.B., Chen, Z., Ryerson, F.J., Kidd, W.S.F., Wang, X., and Zhou, X., 1997, Did the Indo-Asian collision alone create the Tibetan Plateau?: Geology, v. 25, p. 719–722, https:// doi.org/10.1130/0091-7613(1997)025<0719:DTIACA >2.3,CO:2.
- Nábělek, J., Hetényi, G., Vergne, J., Sapkota, S., Kafle, B., Jiang, M., Su, H., Chen, J., Huang, B., and the Hi-CLIMB Team, 2009. Underplating in the Himalaya-Tibet collision zone revealed by the Hi-CLIMB experiment: Science, v. 325, no. 5946, p. 1371–1374, https://doi.org/10.1126/science.1167719.
- Pan, G.T., Ding, J., Yao, D., and Wang, L., 2004, Geological Map of Qinghai-Xiang (Tibet) Plateau and Adjacent Areas: Chengdu, Chengdu Institute of Geology and Mineral Resources, China Geological Survey, Chengdu Cartographic Publishing House, scale 1:1,500,000.
- Pullen, A., Kapp, P., Gehrels, G.E., Vervoort, J.D., and Ding, L., 2008, Triassic continental subduction in central Tibet and Mediterranean-style closure of the Paleo-Tethys Ocean: Geology, v. 36, p. 351–354, https://doi .org/10.1130/G24435A.1.
- Qi, S.S., Song, S.G., Shi, L.C., Cai, H.J., and Hu, J.C., 2014, Discovery of early Paleozoic eclogite, and its geological significance, in the Xiarihamu-Suhaitu area, western part of the East Kunlun: Acta Petrolei Sinica, v. 30, p. 3345–3356 [in Chinese with English abstract].
- Qi, X.X., Li, H.B., and Wu, C.L., 2005, SHRIMP U-Pb zircon dating for Qiashikansayi granodiorite in the northern Altyn Tagh Mountains and its geological implications: Chinese Science Bulletin, v. 50, p. 440–445 [in Chinese with English abstract], https://doi.org/10.1007/BF02897460.
- Qinghai BGMR, (Bureau of Geology and Mineral Resources), 1991, Regional Geology of Qinghai Province: Beijing, Geological Publishing House, 662 p. [in Chinese with English summary].
- Reid, A.J., Wilson, C.J., and Liu, S., 2005, Structural evidence for the Permo-Triassic tectonic evolution of the

- Yidun arc, eastern Tibetan Plateau: Journal of Structural Geology, v. 27, no. 1, p. 119–137, https://doi.org/10.1016/j.jsg.2004.06.011.
- Ritts, B.D., and Biffi, U., 2000, Magnitude of post–Middle Jurassic (Bajocian) displacement on the central Altyn Tagh fault system, northwest China: Geological Society of America Bulletin, v. 112, no. 1, p. 61–74, https://doi.org/10.1130/0016-7606(2000)112<61:MOPJBD> 2.0.CO:2.
- Robinson, D.M., Dupont-Nivet, G., Gehrels, G.E., and Zhang, Y., 2003, The Tula uplift, northwestern China: Evidence for regional tectonism of the northern Tibetan Plateau during late Mesozoic–early Cenozoic time: Geological Society of America Bulletin, v. 115, p. 35–47, https://doi.org/10.1130/0016-7606(2003)115<0035:TTUNCE >2.0.CO;2.
- Roger, F., Arnaud, N., Gilder, S., Tapponnier, P., Jolivet, M., Brunel, M., and Yang, J., 2003, Geochronological and geochemical constraints on Mesozoic suturing in east central Tibet: Tectonics, v. 22, no. 4, 1037, https://doi .org/10.1029/2002TC001466.
- Roger, F., Jolivet, M., Cattin, R., and Malavieille, J., 2011, Mesozoic–Cenozoic tectonothermal evolution of the eastern part of the Tibetan Plateau (Songpan-Garzê, Longmen Shan area): Insights from thermochronological data and simple thermal modelling, in Gloaguen, R., and Ratschbacher, L., eds., Growth and Collapse of the Tibetan Plateau: Geological Society [London] Special Publication 353, 1, p. 9–25, https://doi.org/10.1144/SP353.2.
- Royden, L.H., 1996, Coupling and decoupling of crust and mantle in convergent orogens: Implications for strain partitioning in the crust: Journal of Geophysical Research–Solid Earth, v. 101, no. B8, p. 17,679–17,705, https://doi.org/10.1029/96JB00951.
- Royden, L.H., Burchfiel, B.C., and van der Hilst, R.D., 2008, The geological evolution of the Tibetan Plateau: Science, v. 321, no. 5892, p. 1054–1058, https://doi .org/10.1126/science.1155371.
- Rumelhart, P.E., Yin, A., Cowgill, E., Butler, R., Qing, Z., and Xiao-Feng, W., 1999, Cenozoic vertical-axis rotation of the Altyn Tagh fault system: Geology, v. 27, no. 9, p. 819–822, https://doi.org/10.1130/0091-7613(1999)027<0819:CVAROT>2.3.CO;2.
- Ryan, W.B., Carbotte, S.M., Coplan, J.O., O'Hara, S., Melkonian, A., Arko, R., Weissel, R.A., Ferrini, V., Goodwillie, A., Nitsche, F., Bonczkowski, J., and Zemsky, R., 2009, Global multi-resolution topography synthesis: Geochemistry, Geophysics, Geosystems, v. 10, Q03014, https://doi.org/10.1029/2008GC002332.
- Shi, W., Wang, F., Yang, L., Wu, L., and Zhang, W., 2018, Diachronous growth of the Altyn Tagh Mountains: Constraints on propagation of the northern Tibetan margin from (U-Th)/He dating: Journal of Geophysical Research–Solid Earth, v. 123, p. 6000–6018, https:// doi.org/10.1029/2017JB014844.
- Sloan, R.A., Jackson, J.A., McKenzie, D., and Priestley, K., 2011, Earthquake depth distributions in Central Asia, and their relations with lithosphere thickness, shortening and extension: Geophysical Journal International, v. 185, no. 1, p. 1–29, https://doi.org/10.1111/j.1365-246X.2010.04882.x.
- Sobel, E.R., and Arnaud, N., 1999, A possible middle Paleozoic suture in the Altyn Tagh, NW China: Tectonics, v. 18, no. 1, p. 64–74, https://doi .org/10.1029/1998TC900023.
- Sobel, E.R., Arnaud, N., Jolivet, M., Ritts, B.D., and Brunei, M., 2001, Jurassic to Cenozoic exhumation history of the Altyn Tagh range, northwest China, constrained by 40Ar/39Ar and apatite fission track thermochronology, in Hendrix, M.S., and Davis, G.A., eds., Paleozoic and Mesozoic Tectonic Evolution of Central and Eastern Asia: From Continental Assembly to Intracontinental Deformation: Geological Society of American Memoir 194, p. 247–267.
- Stacey, J.T., and Kramers, J.D., 1975, Approximation of terrestrial lead isotope evolution by a two-stage model: Earth and Planetary Science Letters, v. 26, no. 2, p. 207– 221, https://doi.org/10.1016/0012-821X(75)90088-6.
- Suppe, J., 1983, Geometry and kinematics of fault-bend folding: American Journal of Science, v. 283, no. 7, p. 684–721, https://doi.org/10.2475/ajs.283.7.684.
- Tapponnier, P., Xu, Z.Q., Roger, F., Meyer, B., Arnaud, N., Wittlinger, G., and Yang, J.S., 2001, Oblique stepwise

- rise and growth of the Tibet Plateau: Science, v. 294, p. 1671–1677, https://doi.org/10.1126/science.105978.
- Taylor, M., and Yin, A., 2009, Active structures of the Himalayan-Tibetan orogen and their relationships to earthquake distribution, contemporary strain field, and Cenozoic volcanism: Geosphere, v. 5, no. 3, p. 199– 214, https://doi.org/10.1130/GES00217.1.
- Tocheport, A., Rivera, L., and Van der Woerd, J., 2006, A study of the 14 November 2001 Kokoxili earthquake: History and geometry of the rupture from teleseismic data and field observations: Bulletin of the Seismological Society of America, v. 96, no. 5, p. 1729–1741, https://doi.org/10.1785/0120050200.
- Vincent, S.J., and Allen, M.B., 1999, Evolution of the Minle and Chaoshui Basins, China: Implications for Mesozoic strike-slip basin formation in Central Asia: Geological Society of America Bulletin, v. 111, no. 5, p. 725–742, https://doi.org/10.1130/0016-7606(1999)111<0725:EO TMAC>2.3.CO;2.
- Wang, C., Liu, L., Zhang, A.D., Yang, W.Q., and Cao, Y.T., 2008a, Geochemistry and petrography of early Paleozoic Yusupuleke Tagh rapakivi-textured granite complex, South Altyn: An example for magma mixing: Acta Petrologica Sinica (Yanshi Xuebao), v. 24, no. 12, p. 2809–2819 [in Chinese with English abstract].
- Wang, C.S., Zhao, X.X., Liu, Z., Lippert, P.C., Graham, S.A., Coe, R.S., and Li, Y., 2008b, Constraints on the early uplift history of the Tibetan Plateau: Proceedings of the National Academy of Sciences of the United States of America, v. 105, no. 13, p. 4987–4992, https://doi .org/10.1073/pnas.0703595105.
- Wang, C.S., Gao, R., Yin, A., Wang, H., Zhang, Y., Guo, T., and Li, Y., 2011, A mid-crustal strain-transfer model for continental deformation: A new perspective from high-resolution deep seismic-reflection profiling across NE Tibet: Earth and Planetary Science Letters, v. 306, no. 3-4, p. 279–288, https://doi.org/10.1016/ j.epsl.2011.04.010.
- Wang, E., 1997, Displacement and timing along the northern strand of the Altyn Tagh fault zone, northern Tibet: Earth and Planetary Science Letters, v. 150, no. 1-2, p. 55–64, https://doi.org/10.1016/S0012-821X(97)00085-X.
- Wang, F., Shi, W., Zhang, W., Wu, L., Yang, L., Wang, Y., and Zhu, R., 2017, Differential growth of the northern Tibetan margin: Evidence for oblique stepwise rise of the Tibetan Plateau: Scientific Reports, v. 7, p. 41164, https://doi.org/10.1038/srep41164.
- Wang, L., Johnston, S.T., and Chen, N., 2019, New insights into the Precambrian tectonic evolution and continental affinity of the Qilian block: Evidence from geochronology and geochemistry of metasupracrustal rocks in the North Wulan terrane: Geological Society of America Bulletin (in press), https://doi.org/10.1130/B35059.1.
- Wang, L.Q., Pan, G.T., Ding, J., and Yao, D.S., compiler, 2013, Geological Map of the Tibetan Plateau at a Scale of 1:1.5 M with Explanations: Beijing, Geological Publishing House, 288 p.
- Wu, C., Yin, A., Zuza, A.V., Zhang, J.Y., Liu, W.C., and Ding, L., 2016a, Pre-Cenozoic geologic history of the central and northern Tibetan Plateau and the role of Wilson cycles in constructing the Tethyan orogenic system: Lithosphere, v. 8, p. 254–292, https://doi.org/10.1130/ L494.1.
- Wu, C., Zuza, A.V., Yin, A., Liu, C.F., Reith, R.C., Zhang, J.Y., Liu, W.C., and Zhou, Z.G., 2017, Geochronology and geochemistry of Neoproterozoic granitoids in the central Qilian Shan of northern Tibet: Reconstructing the amalgamation processes and tectonic history of Asia: Lithosphere, v. 9, no. 4, n. 609–636.
- Asia: Lithosphere, v. 9, no. 4, p. 609–636.
 Wu, C., Zhou, Z.G., Zuza, A.V., Wang, G.S., Liu, C.F., and Jiang, T., 2018, A 1.9-Ga mélange along the northern margin of the North China craton: Implications for the assembly of Columbia supercontinent: Tectonics, v. 37, no. 10, p. 3610–3646, https://doi.org/10.1029/2018TC005103.
- Wu, C., Zuza, A.V., Chen, X.H., Ding, L., Levy, D.A., Liu, C.F., Liu, W.C., Jiang, T., and Stockli, D.F., 2019a, Tectonics of the Eastern Kunlun Range: Cenozoic reactivation of a Paleozoic–early Mesozoic orogen: Tectonics, v. 38, no. 5, p. 1609–1650.
- Wu, C., Zuza, A.V., Zhou, Z.G., Yin, A., McRivette, M.W., Chen, X.H., Ding, L., and Geng, J.Z., 2019b, Mesozoic–Cenozoic evolution of the Eastern Kunlun Range,

- central Tibet, and implications for basin evolution within the Indo-Asian collision: Lithosphere, v. 11, no. 4, p. 524–550, https://doi.org/10.1130/L1065.1.
- Wu, C.L., Yao, S.Z., Zeng, L.S., Yang, J.S., Wooden, J.L., Chen, S.Y., and Mazadab, F.K., 2006, Bashikaogong– Shimierbulake granitic complex, north Altun, NW China: Geochemistry and zircon SHRIMP ages: Science in China, ser. D, Earth Sciences, v. 49, p. 1233–1251, https://doi.org/10.1007/s11430-006-2041-6.
- Wu, C.L., Yang, J., Robinson, P.T., Wooden, J.L., Mazdab, F.K., Gao, Y., and Chen, Q., 2009, Geochemistry, age and tectonic significance of granitic rocks in north Altun, northwest China: Lithos, v. 113, no. 3-4, p. 423– 436, https://doi.org/10.1016/j.lithos.2009.05.009.
- Wu, C.L., Gao, Y.H., Lei, M., Qin, H.P., Liu, C.H., Li, M.Z., Frose, B.R., and Wooden, J.L., 2014a, Zircon SHRIMP U-Pb dating, Lu-Hf isotopic characteristics and petrogenesis of the Paleozoic granites in Mangya area, southern Altun, NW China: Acta Petrologica Sinica (Yanshi Xuebao), v. 30, no. 8, p. 2297–2323 [in Chinese with English abstract].
- Wu, C.L., Lei, M., Wu, D., Zhang, X., Cheng, H.J., and Li, T.X., 2016b, Zircon U-Pb dating of Paleozoic granite from South Altun and response of the magmatic activity to the tectonic evolution of the Altun orogenic belt: Acta Geologica Sinica, v. 90, p. 2276–2315 [in Chinese with English abstract].
- Wu, L., Xiao, A., Ma, D., Li, H., Xu, B., Shen, Y., and Mao, L., 2014b, Cenozoic fault systems in southwest Qaidam Basin, northeastern Tibetan Plateau: Geometry, temporal development, and significance for hydrocarbon accumulation: American Association of Petroleum Geologists Bulletin, v. 98, no. 6, p. 1213–1234, https:// doi.org/10.1306/11131313087.
- Wu, L., Lin, X.B., Cowgill, E., Xiao, A.C., Cheng, X.G., Chen, H.L., Zhao, H.F., Shen, Y., and Yang, S.F., 2019c, Middle Miocene reorganization of the Altyn Tagh fault system, northern Tibetan Plateau: Geological Society of America Bulletin, v. 131, no. 7-8, p. 1157–1178, https://doi.org/10.1130/B31875.1.
- Wu, S.P., Wu, C.L., and Chen, Q.L., 2007, Characteristics and tectonic setting of the Tula aluminous A-type granite at the south side of the Altyn Tagh fault, NW China: Geological Bulletin of China, v. 26, no. 10, p. 1385– 1392 [in Chinese with English abstract].
- Xi, R.G., Xiao, P.X., and Wu, Y.Z., 2010, The geological significances, composition and age of the monzonitic granite in Kendekeke iron mine: Northwest Geology, v. 43, p. 195–202 [in Chinese].
- Xiao, W., Windley, B.F., Yong, Y., Yan, Z., Yuan, C., Liu, C., and Li, J., 2009, Early Paleozoic to Devonian multipleaccretionary model for the Qilian Shan, NW China: Journal of Asian Earth Sciences, v. 35, no. 3, p. 323– 333, https://doi.org/10.1016/j.jseaes.2008.10.001.
- Xiao, W., Li, S., Santosh, M., and Jahn, B.M., 2012, Orogenic belts in Central Asia: Correlations and connections: Journal of Asian Earth Sciences, v. 49, p. 1–6, https://doi.org/10.1016/j.jseaes.2012.03.001.
- Xinjiang Bureau of Geology and Mineral Resources (BGMR), 1993, Regional Geology of Xinjiang Uygur Autonomous Region: Geological Memoirs of the Ministry of Geology and Mineral Resources: Beijing, P.R. China, Geological Publishing House, 841 p. [in Chinese with English abstract].
- Xinjiang Bureau of Geology and Mineral Resources (BGMR), 2003, Geological Map of Qiemo, Xinjiang, China, scale 1:25,000: Hubei Autonomous Region Regional Geological Survey Institute: Beijing, P.R. China, Geological Publishing House, 350 p. [in Chinese].
- Xiu, Q.Y., Yu, H.F., Liu, Y.S., Lu, S.N., Mao, D.B., Li, H.M., and Li, Q., 2007, Geology and zircon U-Pb age of pillow basalt at Qiashikansoy in northern Altun Tagh, W China: Acta Geologica Sinica, v. 81, no. 6, p. 787–794 [in Chinese with English abstract].
- Xu, X.M., Ding, Z., Shi, D., and Li, X., 2013, Receiver function analysis of crustal structure beneath the eastern Tibetan Plateau: Journal of Asian Earth Sciences, v. 73, p. 121–127, https://doi.org/10.1016/ j.jseaes.2013.04.018.
- Xu, X.M., Niu, F., Ding, Z., and Chen, Q., 2018, Complicated crustal deformation beneath the NE margin of the Tibetan Plateau and its adjacent areas revealed by multi-station receiver function gathering: Earth and

- Planetary Science Letters, v. 497, p. 204–216, https://doi.org/10.1016/j.epsl.2018.06.010.
- Yakovlev, P.V., 2015, Evolution of the Indo-Asian Orogen: Insights from the Deformation of the Northern Tibetan Plateau, Mass Balance Calculations, and Volcanic Geochemistry [Ph.D thesis]: Ann Arbor, Michigan, University of Michigan, 296 p.
- Yang, J.S., Robinson, P.T., Jiang, C.F., and Xu, Z.Q., 1996, Ophiolites of the Kunlun Mountains, China, and their tectonic implications: Tectonophysics, v. 258, p. 215– 231, https://doi.org/10.1016/0040-1951/95)00199-9.
- Yang, J.S., Shi, R.D., Wu, C.L., Su, D.C., Chen, S.Y., Wang, X.B., and Wooden, J., 2008, Petrology and SHRIMP age of the Hongliugou ophiolite at Milan, north Altun, at the northern margin of the Tibetan Plateau: Acta Petrologica Sinica (Yanshi Xuebao), v. 24, no. 7, p. 1567– 1584 [in Chinese with English abstract].
- Yang, W.Q., Liu, L., Ding, H.B., Xiao, P.X., Cao, Y.T., and Kang, L., 2012, Geochemistry, geochronology and zircon Hf isotopes of the Dimunalike granite in South Altyn Tagn and its geological significance: Acta Petrologica Sinica (Yanshi Xuebao), v. 28, p. 4139–4150 [in Chinese with English abstract].
- Yang, Y., and Liu, M., 2009, Crustal thickening and lateral extrusion during the Indo-Asian collision: A 3D viscous flow model: Tectonophysics, v. 465, no. 1-4, p. 128–135, https://doi.org/10.1016/j.tecto.2008.11.002.
- Ye, X.T., Zhang, C.L., Santosh, M., Zhang, J., Fan, X.K., and Zhang, J.J., 2016, Growth and evolution of Precambrian continental crust in the southwestern Tarim terrane: New evidence from the ca. 1.4 Ga A-type granties and Paleoproterozoic intrusive complex: Precambrian Research, v. 275, p. 18–34, https://doi.org/10.1016/ j.precamres.2015.12.017.
- Ye, Z., Gao, R., Li, Q., Zhang, H., Shen, X., Liu, X., and Gong, C., 2015, Seismic evidence for the North China plate underthrusting beneath northeastern Tibet and its implications for plateau growth: Earth and Planetary Science Letters, v. 426, p. 109–117, https://doi .org/10.1016/j.epsl.2015.06.024.
- Yin, A., 2000, Mode of Cenozoic east-west extension in Tibet suggesting a common origin of rifts in Asia during the Indo-Asian collision: Journal of Geophysical Research, v. 105, p. 21,745–21,759, https://doi .org/10.1029/2000JB900168.
- Yin, A., 2010, Cenozoic tectonic evolution of Asia: A preliminary synthesis: Tectonophysics, v. 488, p. 293–325, https://doi.org/10.1016/j.tecto.2009.06.002.
- Yin, A., and Harrison, T.M., 2000, Geologic evolution of the Himalayan-Tibetan orogen: Annual Review of Earth and Planetary Sciences, v. 28, p. 211–280, https://doi.org/10.1146/annurev.earth.28.1.211.
- Yin, A., and Nie, S., 1996, A Phanerozoic palinspastic reconstruction of China and its neighboring regions, in Yin, A., and Harrison, T.M., The Tectonic Evolution of Asia: New York, Cambridge University Press, p. 442–485.
- Yin, A., Harrison, T.M., Murphy, M., Grove, M., Nie, S., Ryerson, F., Feng, W.X., and Le, C.Z., 1999, Tertiary deformation history of southeastern and southwestern Tibet during the Indo-Asian collision: Geological Society of America Bulletin, v. 111, no. 11, p. 1644–1664, https://doi.org/10.1130/0016-7606(1999)111≤1644:TD HOSA≥2.3.CO;2.
- Yin, A., Rumelhart, P., Butler, R., Cowgill, E., Harrison, T., Foster, D., Ingersoll, R., Qing, Z., Xian-Qiang, Z., and Xiao-Feng, W., 2002, Tectonic history of the Altyn Tagh fault system in northern Tibet inferred from Cenozoic sedimentation: Geological Society of America Bulletin, v. 114, no. 10, p. 1257–1295, https://doi.org/10.1130/0016-7606(2002)114≤1257:THOTAT≥2. 0.CO:2.
- Yin, A., Dang, Y., Zhang, M., McRivette, M.W., Burgess, W.P., and Chen, X.H., 2007, Cenozoic tectonic evolution of Qaidam Basin and its surrounding regions (Part 2): Wedge tectonics in southern Qaidam Basin and the Eastern Kunlun Range, in Sears, J.W., et al., eds., Whence the Mountains? Inquiries into the Evolution of Orogenic Systems: A Volume in Honor of Raymond A. Price: Geological Society of America Special Paper 433, p. 369–390, https://doi.org/10.1130/2007.2433(18).
- Yin, A., Dang, Y.Q., Wang, L.C., Jiang, W.M., Zhou, S.P., Chen, X.H., Gehrels, G.E., and McRivette, M.W., 2008a, Cenozoic tectonic evolution of Qaidam Basin

- and its surrounding regions (Part 1): The southern Qilian Shan-Nan Shan thrust belt and northern Qaidam Basin: Geological Society of America Bulletin, v. 120, no. 7-8, p. 813–846, https://doi.org/10.1130/R26180.1
- Yin, A., Dang, Y.Q., Zhang, M., Chen, X.H., and McRivette, M.W., 2008b, Cenozoic tectonic evolution of the Qaidam Basin and its surrounding regions (Part 3): Structural geology, sedimentation, and regional tectonic reconstruction: Geological Society of America Bulletin, v. 120, no. 7-8, p. 847–876, https://doi.org/10.1130/B26232.1.
- Yu, M., Feng, C.Y., Santosh, M., Mao, J.W., Zhu, Y.F., Zhao, Y.M., and Li, B., 2017, The Qiman Tagh orogen as a window to the crustal evolution in northern Qinghai— Tibet Plateau: Earth-Science Reviews, v. 167, p. 103– 123, https://doi.org/10.1016/j.earscirev.2017.02.008.
- Yuan, D.Y., Ge, W.P., Chen, Z.W., Li, C.Y., Wang, Z.C., Zhang, H.P., Zhang, P.Z., Zheng, D.W., Zheng, W.J., Craddock, W.H., Dayem, K.E., Duvall, A.R., Hough, B.G., Lease, R.O., Champagnac, J.D., Burbank, D.W., Clark, M.K., Farley, K.A., Garzione, C.N., Kirby, E., Molnar, P., and Roe, G.H., 2013, The growth of northeastern Tibet and its relevance to large-scale continental geodynamics: A review of recent studies: Tectonics, v. 32, p. 1358–1370, https://doi.org/10.1002/ject_20081
- Yue, Y., Ritts, B.D., Graham, S.A., Wooden, J.L., Gehrels, G.E., and Zhang, Z., 2004, Slowing extrusion tectonics: Lowered estimate of post–early Miocene slip rate for the Altyn Tagh fault: Earth and Planetary Science Letters, v. 217, no. 1-2, p. 111–122, https://doi .org/10.1016/S0012-821X(03)00544-2.
- Yue, Y., Graham, S.A., Ritts, B.D., and Wooden, J.L., 2005, Detrital zircon provenance evidence for large-scale extrusion along the Altyn Tagh fault: Tectonophysics, v. 406, no. 3-4, p. 165–178, https://doi.org/10.1016/ i.tecto.2005.05.023.
- Zhan, Q.Y., Zhu, D.C., Wang, Q., Cawood, P.A., Xie, J.C., Li, S.M., and Zhao, Z.D., 2018, Constructing the eastern margin of the Tibetan Plateau during the Late Triassic: Journal of Geophysical Research–Solid Earth, v. 123, no. 12, p. 10,449–10,459 https://doi.org/10.1029/2018JB016353.
- Zhang, A.D., Liu, L., Sun, Y., Chen, D.L., Wang, Y., and Luo, J.H., 2004, SHRIMP U-Pb dating of zircons and its geological significance from UHP granitoid gneiss in Altyn Tagh: Chinese Science Bulletin, v. 49, p. 2527– 2532, https://doi.org/10.1007/BF03183726.

- Zhang, J.X., Zhang, Z.M., Xu, Z.Q., Yang, J.S., and Cui, J.W., 1999, The ages of U-Pb and Sm-Nd for eclogite from the western segment of Altyn Tagh tectonic belt: Chinese Science Bulletin, v. 44, p. 2256–2259, https:// doi.org/10.1007/BF02885933.
- Zhang, J.X., Zhang, Z.M., Xu, Z.Q., Yang, J.S., and Cui, J.W., 2001, Petrology and geochronology of eclogite from the western segment of the Altyn Tagh, northwestern China: Lithos, v. 56, p. 187–206, https://doi .org/10.1016/S0024-4937(00)00052-9.
- Zhang, J.X., Mattinson, C.G., Meng, F.C., and Wang, Y.S., 2005, An early Paleozoic HP/HT granulite-garnet peridotite association in the South Altyn Tagh, NW China: P-T history and U-Pb geochronology: Journal of Metamorphic Geology, v. 23, p. 491–510, https://doi .org/10.1111/j.1525-1314.2005.00585.x.
- Zhang, J.X., Mattinson, C.G., Meng, F., Wan, Y.S., and Tung, K., 2008, Polyphase tectonothermal history recorded in granulitized gneisses from the North Qaidam HP/ UHP metamorphic terrane, western China: Evidence from zircon U-Pb geochronology: Geological Society of America Bulletin, v. 120, p. 732–749, https://doi. org/10.1130/B26093.1.
- Zhang, L., Unsworth, M., Jin, S., Wei, W., Ye, G., Jones, A.G., and Vozar, J., 2015, Structure of the Central Altyn Tagh fault revealed by magnetotelluric data: New insights into the structure of the northern margin of the India-Asia collision: Earth and Planetary Science Letters, v. 415, p. 67–79, https://doi.org/10.1016/j.epsl.2015.01.025.
- Zhao, J., Mooney, W.D., Zhang, X., Li, Z., Jin, Z., and Okaya, N., 2006, Crustal structure across the Altyn Tagh Range at the northern margin of the Tibetan Plateau and tectonic implications: Earth and Planetary Science Letters, v. 241, no. 3-4, p. 804–814, https://doi.org/10.1016/j.epsl.2005.11.003.
- Zhou, D., and Graham, S.A., 1996, Extrusion of the Altyn Tagh wedge: A kinematic model for the Altyn Tagh fault and palinspastic reconstruction of northern China: Geology, v. 24, no. 5, p. 427–430, https://doi.org/10.1130/0091-7613(1996)024<0427:EOTATW>2.3.CO:2.
- Zhou, H.W., and Murphy, M.A., 2005, Tomographic evidence for wholesale underthrusting of India beneath the entire Tibetan Plateau: Journal of Asian Earth Sciences, v. 25, no. 3, p. 445–457, https://doi.org/10.1016/j.jseaes.2004.04.007.
- Zhu, L.P., and Helmberger, D.V., 1998, Moho offset across the northern margin of the Tibetan Plateau: Science, v. 281, p. 1170–1172, https://doi.org/10.1126/science.281.5380.1170.

- Zhu, L.P., Tan, Y., Helmberger, D.V., and Saikia, C.K., 2006, Calibration of the Tibetan Plateau using regional seismic waveforms: Pure and Applied Geophysics, v. 163, p. 1193–1213, https://doi.org/10.1007/s00024-006-0073-7
- Zhu, W., Wu, C., Wang, J., and Zhou, T., 2019, Provenance analysis of detrital monazite, zircon and Cr-spinel in the northern Tibetan Plateau: Implications for the Paleozoic tectonothermal history of the Altyn Tagh and Qimen Tagh Ranges: Basin Research, v. 31, no. 3, p. 539–561, https://doi.org/10.1111/bre.12333.
- Zuza, A.V., and Yin, A., 2016, Continental deformation accommodated by non-rigid passive bookshelf faulting: An example from the Cenozoic tectonic development of northern Tibet: Tectonophysics, v. 677, p. 227–240, https://doi.org/10.1016/j.tecto.2016.04.007.
- Zuza, A.V., and Yin, A., 2017, Balkatach hypothesis: A new model for the evolution of the Pacific, Tethyan, and Paleo-Asian oceanic domains: Geosphere, v. 13, no. 5, p. 1664–1712, https://doi.org/10.1130/ GES01463.1.
- Zuza, A.V., Cheng, X., and Yin, A., 2016, Testing models of Tibetan Plateau formation with Cenozoic shortening estimates across the Qilian Shan–Nan Shan thrust belt: Geosphere, v. 12, no. 2, p. 501–532, https://doi .org/10.1130/GES01254.1.
- Zuza, A.V., Yin, A., Lin, J., and Sun, M., 2017, Spacing and strength of active continental strike-slip faults: Earth and Planetary Science Letters, v. 457, p. 49–62, https:// doi.org/10.1016/j.epsl.2016.09.041.
- Zuza, A.V., Wu, C., Reith, R.C., Yin, A., Li, J.H., Zhang, J.Y., Zhang, Y.X., Wu, L., and Liu, W.C., 2018, Tectonic evolution of the Qilian Shan: An early Paleozoic orogen reactivated in the Cenozoic: Geological Society of America Bulletin, v. 130, no. 5-6, p. 881–925, https:// doi.org/10.1130/B31721.1.
- Zuza, A. V., Wu, C., Wang, Z.Z., Levy, D., Li, B., Xiong, X.S., and Chen, X.H., 2019, Underthrusting and duplexing beneath the northern Tibetan Plateau and the evolution of the Himalayan-Tibetan orogen: Lithosphere, v. 11, p. 209–231, https://doi.org/10.1130/L1042.1.

SCIENCE EDITOR: BRADLEY S. SINGER ASSOCIATE EDITOR: TIMOTHY KUSKY

MANUSCRIPT RECEIVED 12 JUNE 2019 REVISED MANUSCRIPT RECEIVED 2 AUGUST 2019 MANUSCRIPT ACCEPTED 28 AUGUST 2019

Printed in the US